FIELD MEASUREMENTS AND HYDRODYNAMIC MODELLING TO EVALUATE THE IMPORTANCE OF FACTORS CONTROLLING OVERWASH

Ana Matias[1], Ana Rita Carrasco[1], Carlos Loureiro[1,2,3], Gerd Masselink[4], Umberto Andriolo[5], Robert McCall[6], Óscar Ferreira[1], Theocharis A. Plomaritis[1,7], André Pacheco[1], Martha Guerreiro[8]

[1]CIMA -Universidade do Algarve, Campus de Gambelas, 8000 Faro, Portugal, ammatias@ualg.pt; azarcos@ualg.pt; oferreir@ualg.pt; tplomaritis@ualg.pt; ampacheco@ualg.pt;

[2]Biological and Environmental Sciences, University of Stirling, Stirling, FK9 4LA, U.K.;

[3]School of Agricultural, Earth and Environmental Sciences, University of KwaZulu-Natal, Durban, 4001, South Africa, Loureiroc@ukzn.ac.za;

[4]School of Biological and Marine Sciences, University of Plymouth, PL4 8AA, U.K., g.masselink@plymouth.ac.uk;

[5]INESC -Institute for Systems Engineering and Computers, University of Coimbra, Coimbra, Portugal andriolo.umberto@libero.it;

[6]Deltares, Boussinesqweg 1, Delft 2629 HD, The Netherlands. Robert.McCall@deltares.nl

[7] Faculty of Marine and Environmental Science, Department of Applied Physics, University of Cadiz, Campus Rio San Pedro (CASEM), Puerto Real 11510, Cadiz, Spain

[8]Instituto Hidrográfico, R. das Trinas, 49, 1249-093 Lisboa, Portugal, Martha.Guerreiro@hidrografico.pt;

ABSTRACT

Overwash hydrodynamic datasets are mixed in quality and scope, being difficult to obtain due to fieldwork experimental limitations. Nevertheless, these measurements are crucial to develop reliable models to predict overwash. Aiming to overcome such limitations, this work presents accurate fieldwork data on overwash hydrodynamics, further exploring it to model overwash on a low-lying barrier island. Fieldwork was undertaken on Barreta Island (Portugal) in December 2013, during neap tides and under energetic conditions, with significant wave height reaching 2.6 m. During approximately 4 hours, more than 120 shallow overwash events were measured with a video - camera, a pressure transducer and a current-meter. This high-frequency fieldwork dataset includes runup, overwash number, depth and velocity. Fieldwork data along with information from literature were used to implement XBeach model in non-hydrostatic mode (wave-resolving). The baseline model was tested for six verification cases; the model was able to predict overwash in five. Based in performance metrics and the verification cases, it was considered that the Barreta baseline overwash model is a reliable tool for the prediction of overwash hydrodynamics. The baseline model was then forced to simulate overwash under different hydrodynamic conditions (waves and lagoon water level) and morpho-sedimentary settings (nearshore topography and beach grain-size), within the range of values characteristic for the study area. Based on this study, the order of importance of factors controlling overwash predictability in the study area are: 1^{st}) wave height (more than wave period) can promote overwash 3-4 times more intense than the one recorded during fieldwork; 2^{nd}) nearshore bathymetry, particularly shallower submerge bars, can promote an average decrease of about 30% in overwash; 3^{rd}) grain-size, finer sediment produced an 11% increase in overwash due to reduced infiltration; and 4^{th}) lagoon water level, only negligible differences were evidenced by changes in the lagoon level. This implies that for model predictions to be reliable, accurate wave forecast are necessary and topo-bathymetric configuration needs to be monitored frequently.

Key-words: storm impacts; hydrodynamics; XBeach; runup; nearshore topography; video data.

1. INTRODUCTION

Overwash is the discontinuous transport of seawater and sediment over the barrier crest generated by wave runup (Matias and Masselink, 2017). Overwash episodes during storms are commonly described in the literature, with occurrences associated to offshore significant wave heights ranging from around 4 m (Leatherman, 1976) to more than 9 m (FitzGerald et al., 1994). However, overwash can also occur during non-storm conditions (Matias et al., 2009). Overwash associated with major storms can be catastrophic, but repeated overwash processes are fundamental for long-term natural evolution of transgressive barrier islands, whereby the net volume of sand contained in the barrier structure is often maintained whilst the barrier environments migrate landward (e.g. Dolan and Godfrey, 1973).

Field observations are occasionally carried out during overwash episodes, but most often, such observations are made before and after overwash occurrence (e.g. Cleary et al., 2001; Stone et al., 2004; Stockdon et al., 2009). Overwash field investigations primarily measure morphological changes induced by overwash; yet, only a limited number of studies have also measured overwash hydrodynamics. Moreover, hydrodynamic datasets are mixed in quality and scope, ranging from single hydrodynamic measurements using relatively crude methods (e.g. timing floating objects; Bray and Carter, 1992) to more comprehensive and sophisticated approaches (e.g. laser scanners; Almeida et al., 2017). To overcome logistical and technical field limitations, research efforts have been devoted to the investigation of overwash in laboratory experiments, mainly small-scale experiments (e.g. Figlus et al., 2011; Baldock et al., 2005), but also large-scale experiments (Matias et al., 2012, 2013).

Because field measurements are scarce and difficult to obtain, and laboratory datasets may have scale and applicability limitations, reliable numerical models simulating overwash are valuable to complement field data (e.g. Martins et al., 2017), particularly in extreme wave conditions. More importantly, models can be used as predictive tools, which are crucial to manage coastal areas where overwash is not desirable, to reduce its negative consequences, to assess coastal hotspots and to evaluate and improve coastal defence designs. Recent studies report similar prediction capabilities of runup by using process oriented numerical models and empirical formulations (Vousdouskas et al. 2012; Stockdon et al. 2014; Lerma et al., 2017, Atkinson et al. 2017). Conceptually, if the dominant physical relations are well described, process-based models can provide an improvement over empirical models in conditions that are dissimilar to those used to derive those empirical models, thereby extending the range of conditions and areas of application where predictions can be made. In recent years, advancements have been made in the development and improvement of process-based models for storm impact and overwash on sandy coasts, particularly the XBeach numerical model, developed by Roelvink et al. (2009, 2017). Most overwash validation work has been limited to comparisons of morphological changes (e.g., Lindemer et al., 2010; McCall et al., 2010; De Vet et al., 2015; Muller et al., 2017), and only a few studies have demonstrated XBeach's ability to reproduce hydrodynamic processes (McCall et al., 2014 and Almeida et al., 2017 on gravel barriers and Baumann et al. 2017 on a sandy barrier). Many experimental results have already been collected, but field data of storm events, with well-documented pre-existing conditions, hydrodynamic boundary conditions of waves, wind and surge, and the storm morphological impact measured directly after the storm, are still needed to validate models on the prototype scale (van Dongeren et al., 2017).

In this work, the results of fieldwork measurements during an overwash episode are described in detail, including the hydrodynamic variables, namely waves, tides, overwash flow properties and runup, as well as morphosedimentary measurements such as topography, bathymetry, and grain-size. Using data from the field site, XBeach model was implemented to simulate the observed overwash occurrence, and the model performance for overwash hydrodynamics was evaluated and validated with additional fieldwork measurements. The primary objective of this work is to develop a reliable model for overwash prediction in the study area and to explore the model to evaluate the role of several factors that locally influence overwash hydrodynamics (waves and water levels, nearshore morphology and grain-sizes) on a low-lying barrier island.

2. STUDY AREA

Fieldwork was performed on the western part of Barreta Island, located in the Ria Formosa, southern Portugal (Figure 1), a multi-inlet island system that extends for 55 km along the coast. In December 2013, the field site was located about 1300 m downdrift from Ancão Inlet (Figure 1), which has a northwest to southeast migration trend with very fast rates (40-200 m/year; Vila-Concejo et al., 2002) and was migrating towards the fieldwork site between 1997 and 2015. The fieldwork site is only about 300 m from the easternmost known position of Ancão Inlet since

1947 (Vila-Concejo et al., 2006). The evolution of Ancão Inlet and Barreta Island are strongly interconnected, with low-volume island states associated with sediment starvation due to the updrift trap effect of the inlet (Matias et al., 2009), while high-volume states at Barreta Island relate to the incorporation of swash bars from the inlet ebb-delta (Vila-Concejo et al., 2006). At the fieldwork site, dune vegetation development on small incipient dunes was noted since 2001, with remnants still visible close to the backbarrier (Figures 1 and 2).

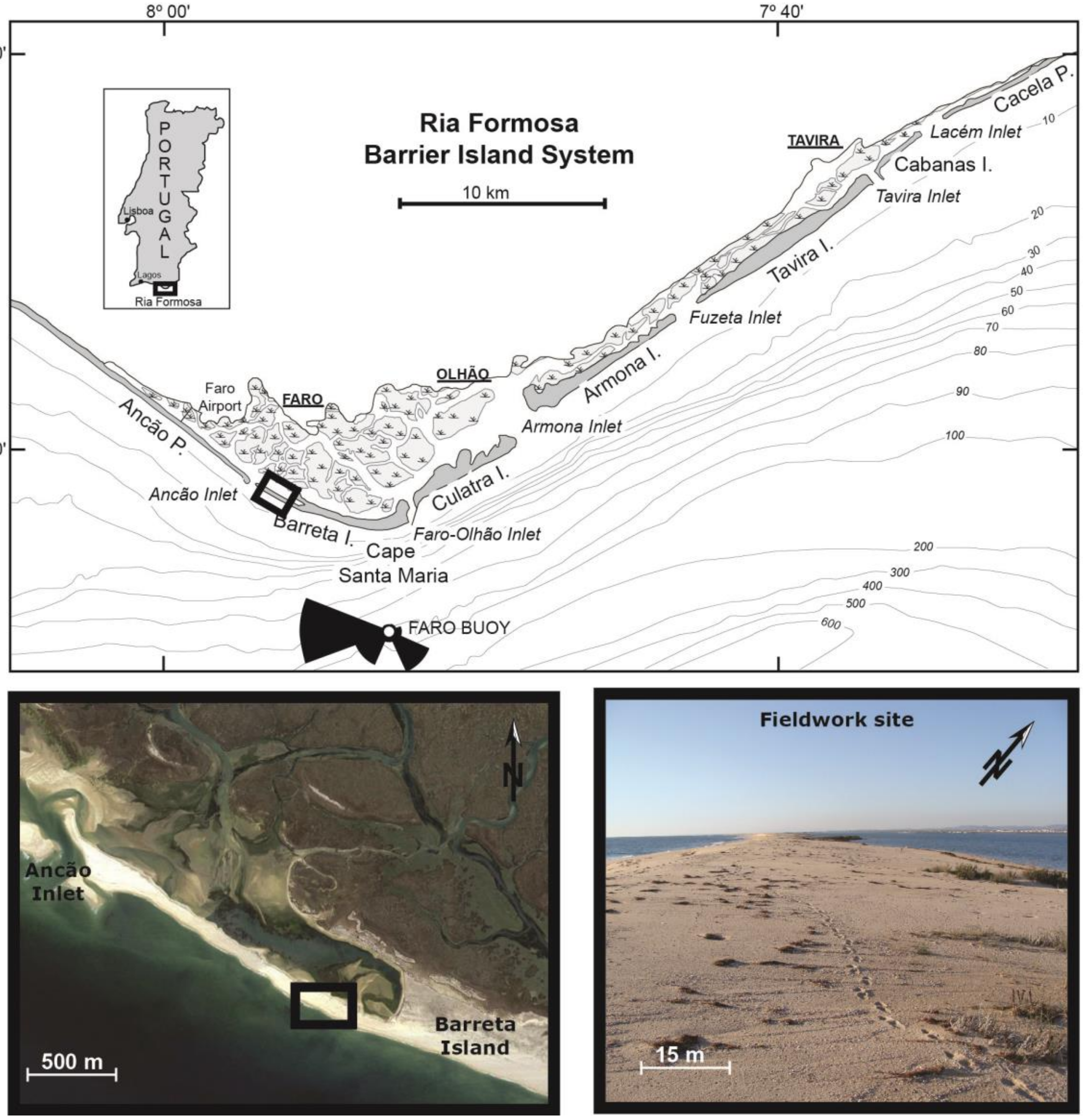

Figure 1 – Top: Fieldwork location within the Ria Formosa barrier island system, Algarve, Portugal. Bottom left: Aerial photograph from 2013 showing the study area location on the Western part of Barreta Island, and Ancão Inlet. Bottom right: Ground picture of the study area looking Westwards, with the lagoon and mainland to the right-hand side.

The Ria Formosa barrier system is in a mesotidal regime, with a mean tidal range of about 2 m that can reach up to 3.5 m during spring tides. The return period of a storm surge with a water level of 2.23 m above Mean Sea Level (MSL) in Lagos (70 km west of the study area) is 10 years (Gama et al., 1994). The offshore wave climate in this area is dominated by W-SW waves (71% of occurrences), while short-period SE waves generated by regional winds occur during 23% of the time (Costa et al., 2001). Wave energy is moderate with an average annual significant wave height (H_s) of 1.0 m and average peak period (T_p) of 8.2 s (Costa et al., 2001). Storm events in the region were define as events with H_s above 3 m (Pessanha and Pires, 1981). According to Costa et al. (2001), a storm from West with H_s of 3–5 m has an annual probability of 0.2% for T_p = 7-11 s, and of 0.1% for T_p = 11-15 s. The western section of Barreta Island has a NW-SE orientation, such that it is directly exposed to W-SW waves, and it is relatively protected from SE waves (Figure 1).

3. FIELDWORK MEASUREMENTS

A fieldwork campaign was conducted at the study site during a period expected to lead to overtopping based on storm wave forecasts and previous knowledge of barrier morphology. During this campaign, which took place on the 12th of December 2013, data was collected between 08:00 and 13:00, when an overwash episode was observed. Measurements were undertaken along a single cross-shore profile in a low-lying section of the barrier, where overwash was expected to occur (Figures 1 and 2A). The selected profile is located on bare sand, but westwards there are remnants of former dunes (Figure 2E), where a control station and campsite were placed and the GPS base unit established.

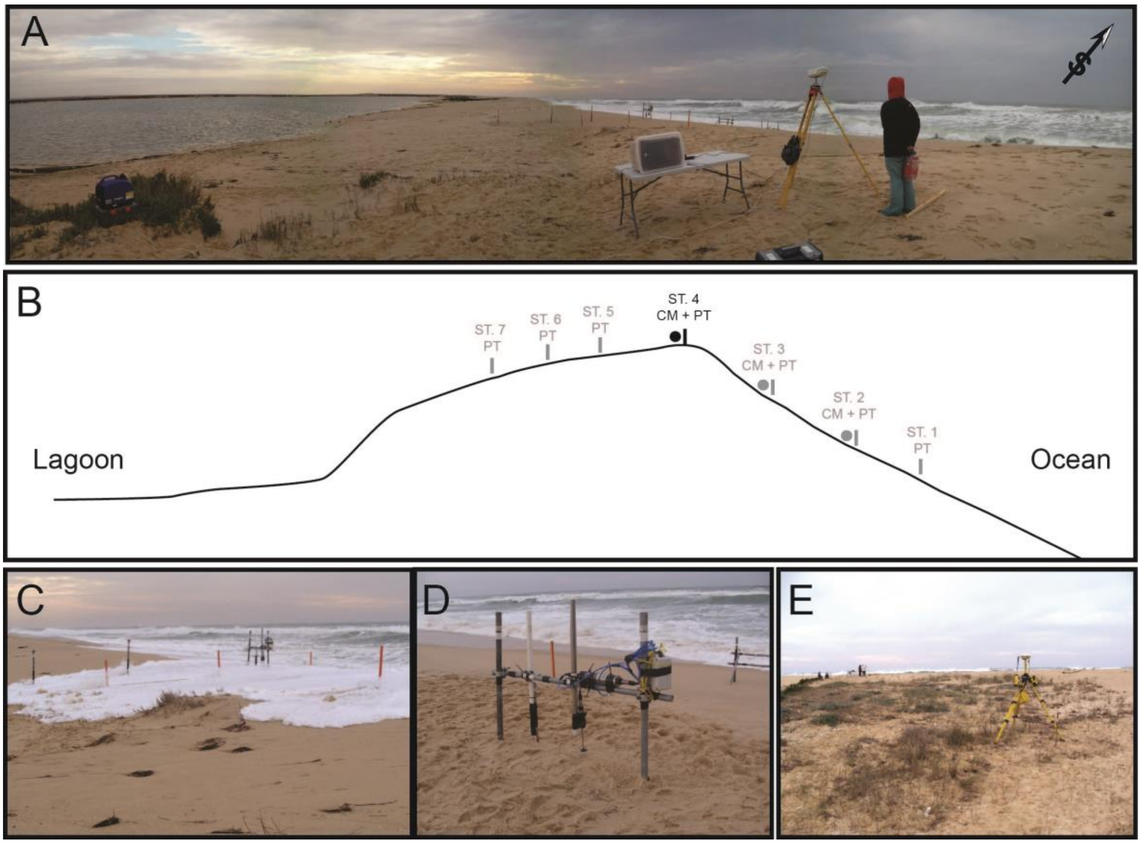

Figure 2 – Fieldwork settings. A: Overview of barrier measuring stations and video monitoring system. B: Location of measuring stations across the barrier island. C: Overwash over the barrier crest, with water reaching stations ST4, ST5, and ST6. D: Detail of measuring station ST4, with the electromagnetic current-meter and data-logger (right hand-side) and the pressure transducers (left-hand side). E: View over the remnants of dune vegetation located westward of the measuring profile, and the base unit of the DGPS.

3.1. OFFSHORE AND NEARSHORE WAVES AND TIDES

Offshore waves during the fieldwork campaign were recorded by a directional wave buoy (Datawell Waverider), operated by the Hydrographic Institute of the Portuguese Navy, and located approximately 8 km from the fieldwork site in 93 m water depth (Figure 1). The wave spectrum was computed internally for sequential periods of 30 minutes and transmitted to a land station, where it was quality checked. To obtain the wave conditions in the nearshore area of the study site, the numerical wave propagation model SWAN (Simulating WAves Nearshore; Booij et al., 1999; Ris et al., 1999) was used. SWAN was run in third generation, 2D stationary mode, and implemented using a nested modelling scheme, with two model domains composed by a 20-m resolution local grid, nested into the 50-m resolution regional grid. Simulations were forced at the offshore boundary of the regional grid with the measured 2D spectra from the wave buoy, variable water levels and wind forcing obtained from the nearby Faro Airport (location in Figure 1). SWAN's default parameters for wave growth, whitecapping dissipation, depth-induced breaking according to the β-kd model for surf-breaking (Salmon and Holhuijsen, 2015), triad and quadruplet wave-wave interactions, were used for all simulations. Bottom friction dissipation was included using the model of Smith et al. (2011), which considers bottom friction as dependent on the formation of seabed ripples and sediment size (set according to measurements in the area; section 3.3).

Tidal levels in the ocean margin were calculated with an algorithm developed by Pacheco et al. (2014); which computes the astronomical constituents with a tidal-analysis toolbox (Pawlowicz et al., 2002) over an hourly time-series for the period 2003–2010 from a tide gauge located on Faro-Olhão Inlet (about 6 km eastwards of the study area; Figure 1). Tidal levels on the lagoon margin were determined using an estimate of the time delay and level shift between oceanic and lagoon tidal levels for this area. The delay and shift were calculated from water level data collected by Popesso et al. (2016). Storm surge values, which were small during this event compared to the astronomic tide, were obtained from the closest operational tidal gauge located in Huelva, Spain (60 km to the East; Puertos de Estado; url: http://www.puertos.es/es-es/oceanografia).

3.2. OVERWASH HYDRODYNAMICS AND RUNUP

The field monitoring system was composed of seven measuring stations (ST) with sets of instruments (current-meters CM and pressure transducers PT) deployed along a cross-shore profile (Figure 2B). Stations were numbered from the low-tide water level at the beach (ST 1 in Figure 2) to the barrier crest (ST 4; Figures 2C and 2D) ending at the backbarrier section, above the lagoon high-water level (ST 7). PTs measuring at 4 Hz were placed at all STs and CMs were placed at ST 2, ST 3 and ST 4. Due to intense erosion during high-tide, ST1 and ST 2 collapsed and ST 3 was damaged. The only operational current meter for the entire duration of the campaign was an electromagnetic current meter (Midas from Valeport, with measuring range 0 – 5 ms^{-1}) at ST 4 (located on the barrier crest). This means that it was impossible to record in-situ swash depth and velocity at the beach face.

During the measured overwash episode a number of overwash events, defined as a single passage of water above the barrier crest, were recorded. Since all instruments were synchronized and calibrated for atmospheric pressure in the field, overwash events were identified and isolated using time tagging. Overwash depths for each event were determined using pressure data from the PT measuring stations and overwash event velocity at crest computed from the electromagnetic CM data. Maximum overwash depth and peak velocity at the barrier crest were calculated for each overwash event. Decreasing overwash depth landward of the barrier crest (from PTs at stations ST5, ST6, and ST7) were discarded, as measurements failed the quality checks. This is likely due to technical limitations in measuring intermittent, short duration, very shallow flows (estimation of less than 5 mm), which characterize overwash events at these locations.

The overwash episode was also monitored by a video camera, acquiring imagery at 10 Hz, mounted on a tripod looking sideways at the instrumented cross-shore profile (Figure 2A). The elevation of the camera sensor was 4.9 m above MSL. All instruments and Ground-Control Points (GCP; red poles in Figure 2C as examples) for video analysis were geo-referenced with an RTK-DGPS (Real Time Kinematics Differential Global Positioning System; Figure 2E).

Image frames were extracted from the video at the same acquisition frequency (i.e. 10Hz) resulting on approximately 170000 images (1600x1200 pixel resolution). The camera intrinsic parameters were determined with the Camera Calibration Toolbox of Bouguet (2007) to correct lens-induced distortions on the images. Overwash Timestack images were produced sampling the pixel array (0.1 m spatial resolution) located along the instrumented barrier profile over the image sequence, and considering sampling periods of 10 minutes (Figure 3 as an example). On the Timestacks images the overwash water front was visible as white stripe line, which was automatically detected based on pixel intensity variation. The average leading-edge velocity of each overwash event on the barrier was estimated through the intersection of the detected water line with instruments' positions, and Timestack-based leading edge velocity was compared to flow velocity obtained with the current meter.

Runup Timestack images were generated between low tide water level and the barrier crest positions during the 3.5 hours of video acquisition. To extract the runup elevation for each swash event, the maximum of the visual edge of the water excursion was manually digitized, on each of the georeferenced 22 Timestack imagesdatasets. The cross-shore distances (swash) were then converted into elevations (runup referred to MSL), using the interpolated barrier profiles corresponding to each 10-min Timestack images with 0.1 m cross-shore resolution (following procedures that can be found e.g. in Vousdoukas et al., 2011; Blenkinsopp et al., 2015; Andriolo et al., 2018). Number of runup values varied between a minimum of 45 to a maximum of 60 values per Timestack over the dataset. Because there is a certain degree of subjectivity in the manual digitizing of runup, an analysis of operator variability was made. Four experienced coastal researchers were asked to independently mark the maximum swash of all events, on the 22 Timestack image datasets (Figure 3, as an example). The Kruskal-Wallis test was used to test the hypothesys that the runup results obtained by the several operators were significantly different. The test indicated that there is a 95% probability that the results obtained by the operators are not statistically different. Based on average results of runup obtained by the four operators, the 2% exceedance runup (R_2), the 10% exceedance runup (R_{10}) and the significant runup (R_{sig}, the average of the top third of runup values) were calculated. The runup statistics were computed assuming a normal distribution fit, which was found to consistenly represent runup distribution by similar previous works (e.g., Stockdon et al., 2006; Hughes et al., 2010; Atkinson et al., 2017).

In summary, across the beach face only runup measurements were obtained from Timestack imagery; at the barrier crest overwash depth was recoded by a PT and the velocity obtained from electromagnetic current meter and from Timestack imagery; and at the barrier top, the overwash water intrusion distance was extracted from Timestack images also. This substantial reduction from the initial seven field stations was related to the intense erosion on the beach face, which led to the collapse of the supporting structures fall and subsequent loss of equipment, to equipment damage when exposed to the turbulent swash zone, and the impossibility of manual measurements of bed variations (for example on rods) on stations 5, 6 and 7 due to the high frequency of overwash during high-tide (about 1 event per minute).

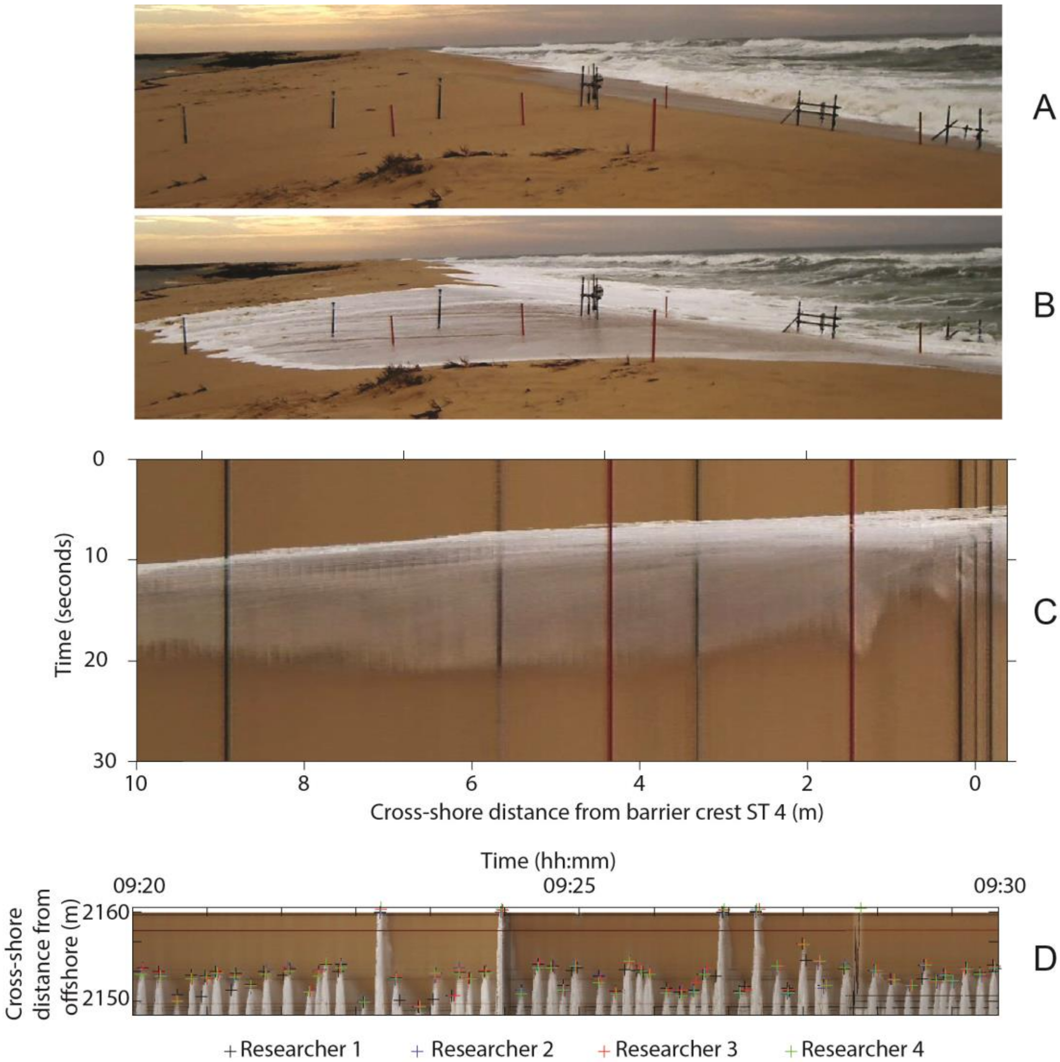

Figure 3 – A and B. Undistorted and cropped images obtained from post-processing video imagery at two timings of an overwash event. C. Timestack with an overwash event produced over 30 seconds. Stations are visible as black vertical lines (ST4 at the crest, on the right, is represented by three black lines, one for each pole and one for the CM) and control points as red lines (red poles). C. Example of runup marking by different researchers on a 10-min Timestack.

3.3. TOPOGRAPHY, BATHYMETRY AND GRAIN-SIZE

Barrier morphology was measured before (at 5:30) and after (at 13:00) the overwash episode (from 08:40 to 12:20) using an RTK-DGPS. Cross-shore profiles during the overwash event were impossible to obtain, therefore profiles were interpolated from the initial and final profiles. Topographic bed changes for each 10-min were obtained by weighting the overall bed change by the percentage of overwash events that occurred during each 10-min.

Offshore bathymetry of the inner-shelf of the study area, from the shoreline to depths of approximately MSL-25 m and extending for about 5 km roughly centred in the fieldwork site, was collected using a survey-grade single beam echo sounder (Odom Ecotrac CV100). Precise positioning and real-time tide correction were obtained using an RTK-DGPS and all data were synchronized and processed with Hypack software (further details on the acquisition system are provided in Horta et al., 2014). Bathymetric surveys were performed on multiple occasions from June 2012 to April 2013, including both pre and post-overwash conditions. Data from the dedicated surveys were combined with offshore bathymetric data provided by the Hydrographic Institute of Portugal to create a bathymetric grid extending from the shoreline to the location of the Faro offshore wave buoy (Figure 4). Bathymetric grids were produced in Surfer software, using Kriging interpolation and considering a linear semi-variogram model. Additionally, cross-shore profiles to be used as input on the XBeach model were interpolated for a 500 m-wide section centred on the fieldwork site and extending, in the cross-shore dimension, for more than 2,000 m from the backbarrier to a depth of MSL -15 m.

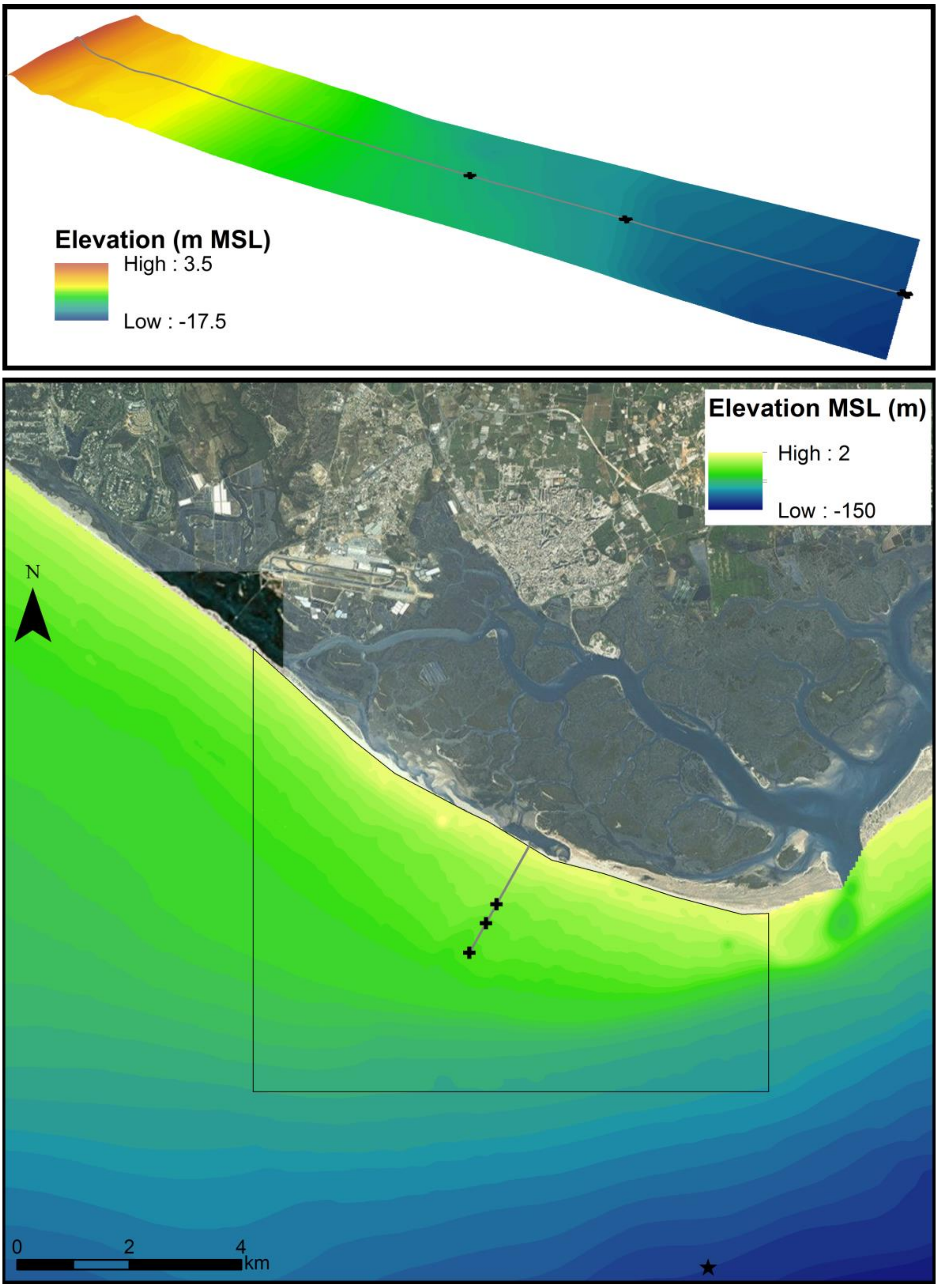

Figure 4 – Location and bathymetry of grids used in wave modelling. Upper panel - high-resolution grid of the cross-shore section centered on the fieldwork site profile (grey line), with locations of depths MSL-12, -15 and -17 m (black crosses) for reference. Lower panel - bathymetry of the 50m-resolution regional grid, with extent of the 20 m-resolution nested local grid (black polygon). Black star indicates the location of the offshore directional wave buoy.

Surficial sediment samples were collected at all stations after the overwash episode. Samples were analysed using traditional laboratory dry sieving procedures for unconsolidated clastic sediments. Sieving was done for sediment grain-sizes between 31.5 mm and 0.063 mm. Percentiles D_{10}, D_{50} (median), and D_{90} were determined using GRADISTAT (Blott and Pye, 2001). Sediment porosity was determined in the laboratory from the void volume ratio of samples.

Further information on the study site grain-size variability was obtained from previous measurements on beaches, dunes and washovers near the study area described in Matias et al. (2009). Information of the nearshore sediment grain-size was obtained from a systematic study of sediments from the inner shelf of the Ria Formosa barrier system published in Rosa et al. (2013).

4. FIELDWORK RESULTS

4.1. HYDRODYNAMICS

During the fieldwork campaign, which occurred during neap tides, tidal levels reached a maximum of about MSL +0.9 m on the ocean side, between 10:00 and 10:30, whilst lagoon tidal elevations varied between 0.17 m and -0.3 m MSL (Figure 5A). Storm surge was almost insignificant, ranging between 0.00 m and 0.06 m. Offshore waves measured by the Waverider buoy averaged 2.5 m, with the highest H_s of 2.64 m recorded at 11:00 (close but not exceeding the storm threshold for this area, 3.0 m).

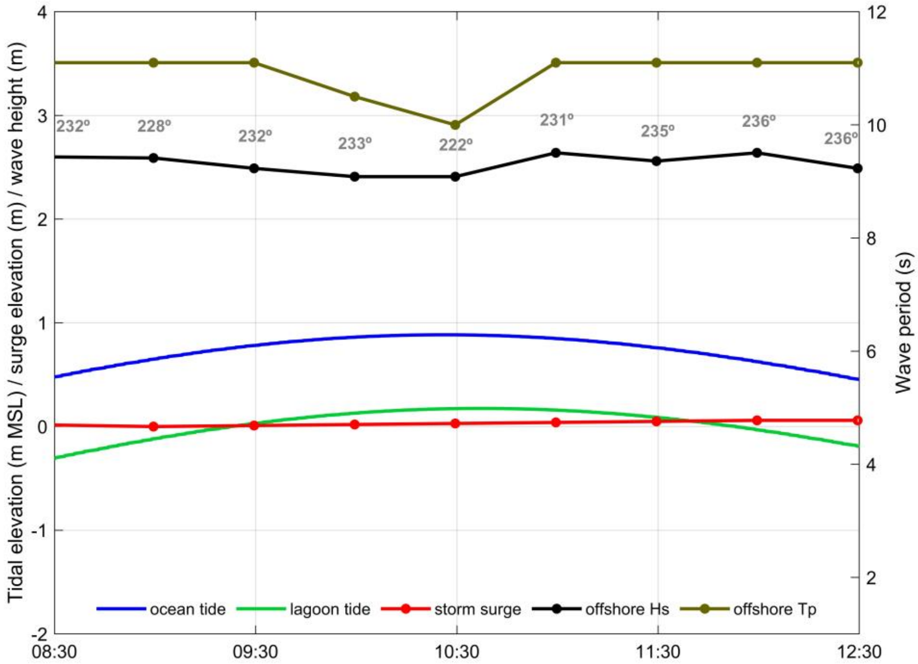

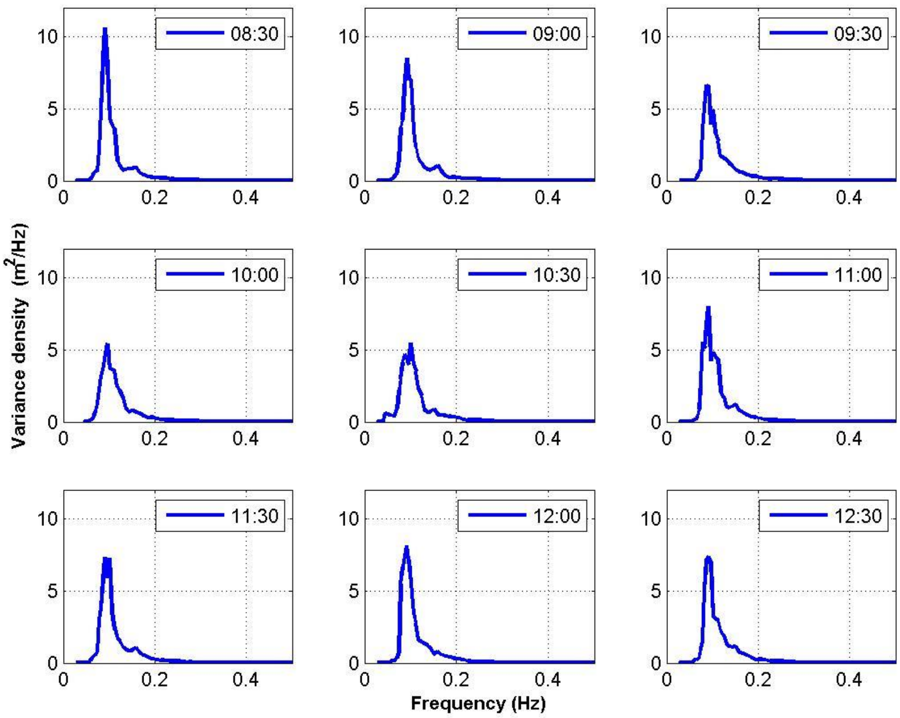

Figure 5 – A. Synthesis of oceanographic conditions during the overwash episode on 12/12/2013. B. Modelled nearshore wave spectra at a depth of MSL-15 m.

At about MSL-12 m depth, wave refraction and bed friction had reduced H_s to 2.0 m – 2.2 m. Waves approached mainly from a SW direction, with an offshore incident angle always smaller than 30 degrees, and a nearshore angle smaller than 12 degrees. During most of the overwash episode, wave spectra were relatively broad in frequency, slightly narrower at the beginning (8:30; Figure 5B and 6A). The highest wave energy peak was associated with wave frequencies around 0.09 Hz, with a second mode around 0.11 Hz. Although several and variable peaks in wave spectra were recorded offshore, two main sets of waves could be identified on the SWAN model output at the MSL-15 m depth. The bi-modal shape of most of the modelled wave spectra, indicates the combination of two wave fields and curve-fitting with various JONSWAP spectra suggests that these two wave fields are characterised by Hs = 2 m and Tp of 11.3 s, and Hs = 1.3 m and Tp of 8.8 s.

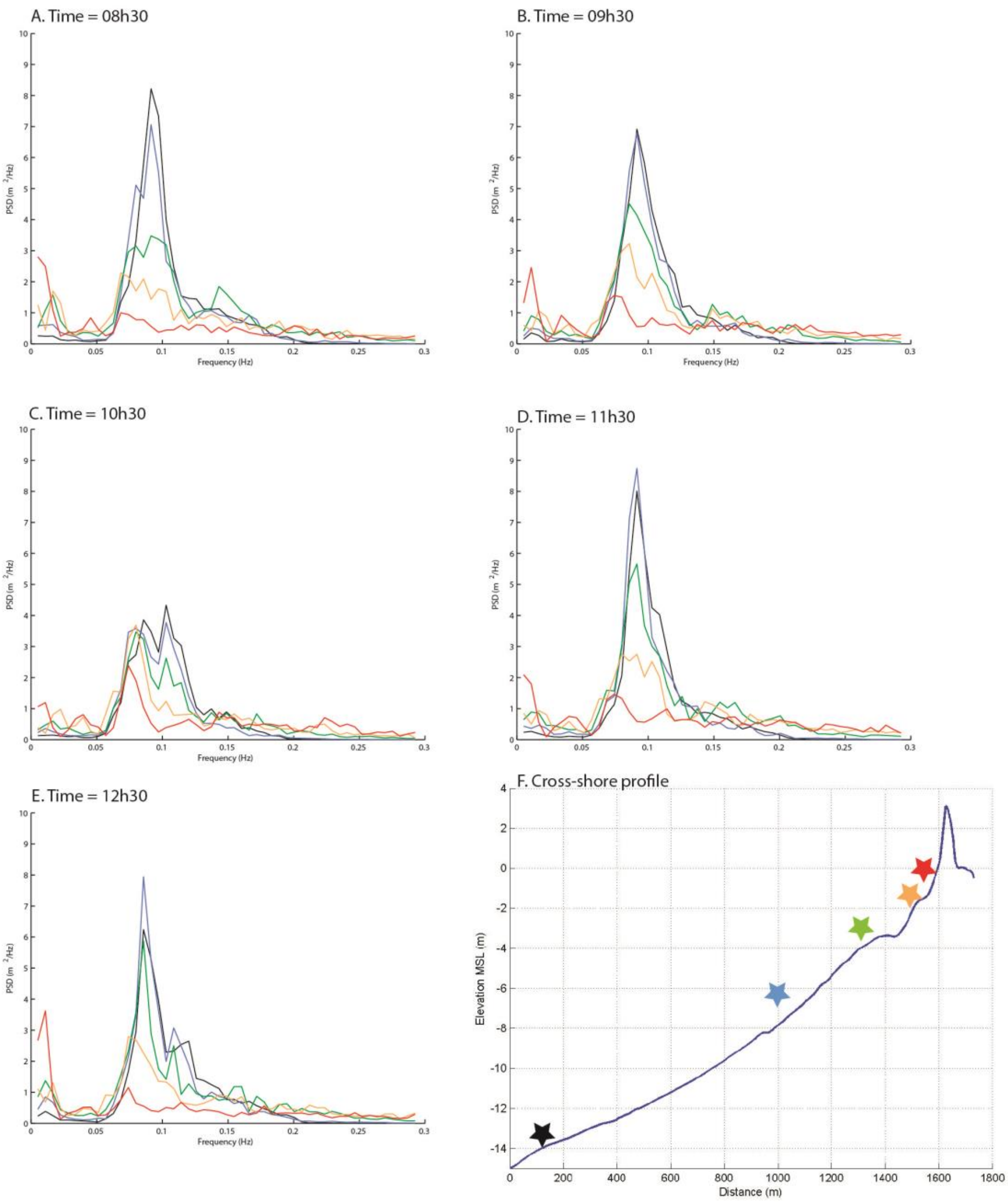

Figure 6 – Example of the transformation of the wave spectra modelled across the offshore and nearshore profile for several time-steps (08h30, 09h30, 10h30, 11h30 and 12h30, for panels A to E, respectively). Stars on the cross-shore profile (panel F) represent the location where the spectra were extracted, and star colours corresponds to line colour of spectra represented in panels A to E.

Runup elevation during the overwash episode is a main parameter controlling the variation and number of overwash events. At the peak of high-tide (10:30) runup parameters R_2 and R_{10} are identical (Figure 7) and coincide with the level of the barrier crest. R_{sig} is more variable but still dominantly influenced by overwash;

values do not increase significantly during high-tide because swash up-slope motion is limited.

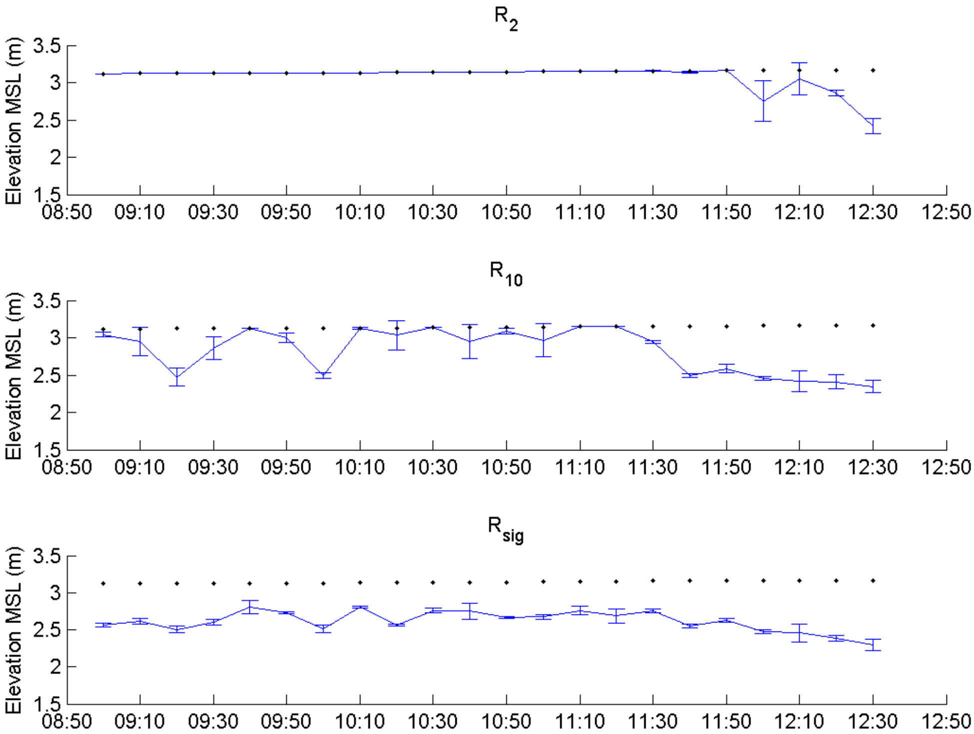

Figure 7 – Statistics of runup during the entire overwash episode. R2 is the 2% exceedance of runup, R10 is the 10% exceedance runup and Rsig is the significant runup (i.e.,). The barrier crest elevation is represented by the black dots. The error bars are the standard deviation of each 10-min runup measurement, considering the results from four operators.

During the surveyed overwash episode a number of overwash events, defined as a single passage of water above the barrier crest, occurred. For more than 4 hours, circa 120 overwash events occurred over the barrier crest were measured at the instrumented cross-shore profile. About 70% of these overwash events occurred between 09:45 and 11:45 (Figure 8). Most overwash events had limited inland intrusion (< 2 m) beyond the crest of the barrier; yet, some events reached the backbarrier lagoon. Peak overwash flow velocity was generally between 1 and 3 m s-

^{1}, although maximum velocities reached values close to 5 m s^{-1} (maximum 5.1 m s^{-1} measurement by the current meter and 4.7 m s^{-1} from video imagery) Average overwash leading edge velocity obtained with video imagery was 2.1 ms^{-1}, similar to the average overwash velocity 1.9 ms^{-1} measured by EM current meter. Overwash flow was very shallow (Figure 8), with mean depth of 0.07 m. These characteristics are typical of overwash flows, which are generally supercritical (according to data compiled by Matias and Masselink, 2017). Larger overwash events had deeper and faster flows, as well as longer durations and larger intrusion distances. Despite the reduction in number of events at the start and end of the fieldwork campaign and variable peak velocities, depths of overwash flows were relatively constant (Figure 8).

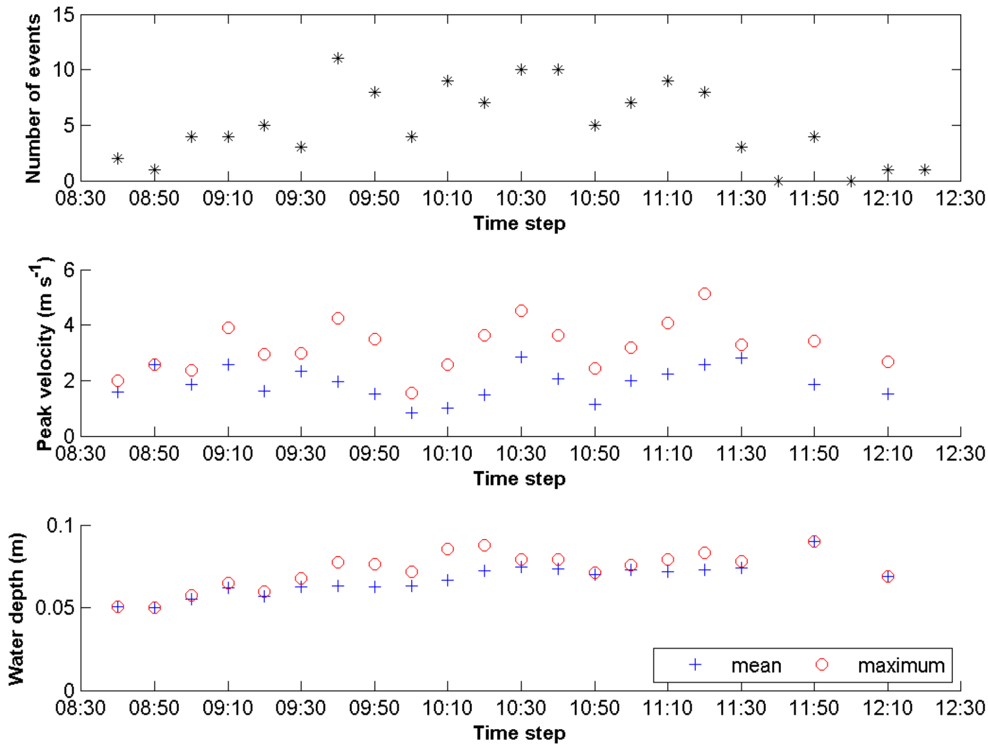

Figure 8 – Overwash events average properties during the entire overwash episode, obtained from the video Timestacks (velocity) and PT (depth) at ST 4 (see Figure 2 for location).

4.2. MORPHOLOGY AND GRAIN-SIZE

During the overwash episode, the beach face was eroded and sand accumulated on the barrier top and farther inland across the barrier (Figure 9). The beach face is steep (average slope of 0.1), with average beach D_{50} (median grain-size) of 0.61 mm (Table 1). The backbarrier surface facing the lagoon has variable slope, exhibiting a coarsening grain-size and a poorer sorting due to the presence of overwash debris lines. Barrier porosity is mostly around 0.3 with a maximum of 0.36 close to ST7 (location on Figure 2). According to data from Matias et al. (2009), at the western part of Barreta Island the average beach D_{50} is 0.65 mm, varying between 0.47 mm and 0.89 mm. In the nearshore area, the average D_{50} is 0.36 mm, whilst offshore sediments became coarser (average D_{50} = 0.43 mm, according to Rosa et al., 2013).

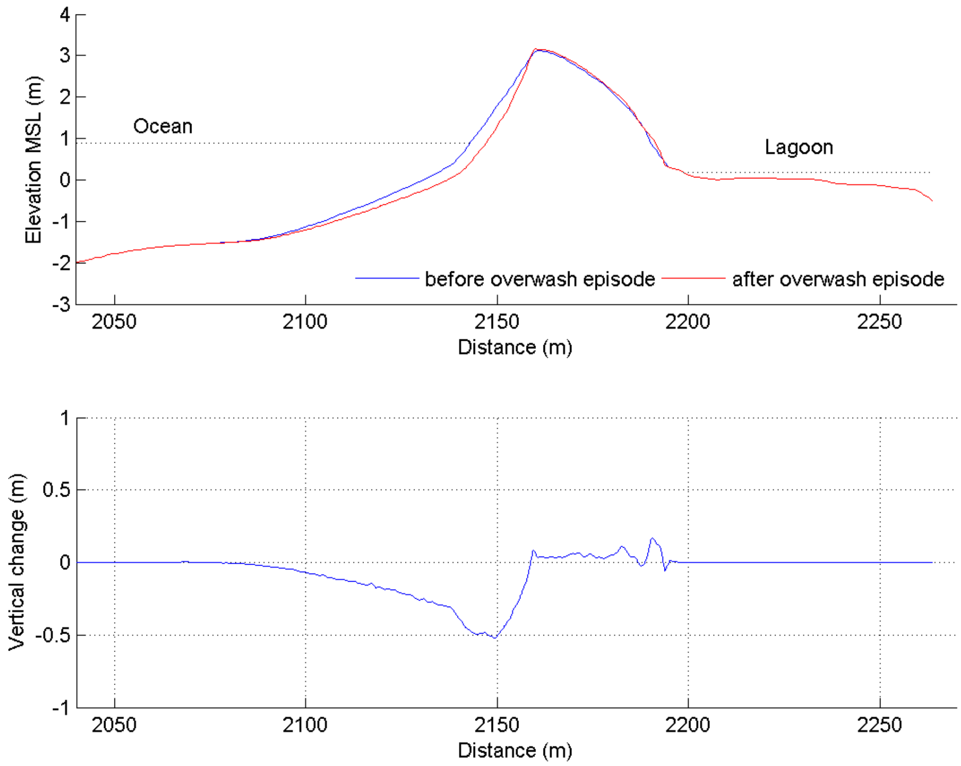

Figure 9 – Topographic profiles of the barrier before and after the overwash episode. The dashed line represents the maximum ocean and lagoon tidal levels. On the lower panel are represented the morphologic variations across the barrier profile during the overwash episode.

Observed changes indicate that the volume of barrier erosion was greater than the volume of overwash induced deposition. The net sediment balance is -13.7 m^3m^{-1}, with only about 1.8 m^3m^{-1} of overwash deposition on the barrier. The net loss of sediment is either attributed to longshore sediment transport or offshore sediment transport to areas below the topographic survey. The topography at the end of the overwash episode was only surveyed down to MSL -1 m on the ocean margin; below this depth, a former nearshore survey was used to reconstruct the barrier morphology. The nearshore area, between MSL -1 m and -3.5 m typically exhibits a sandbar that changes in morphology and elevation through time (Figure 10). It is possible that cross-shore sediment transport during this event while contributing to sandbar formation, led to offshore sediment loss from the barrier.

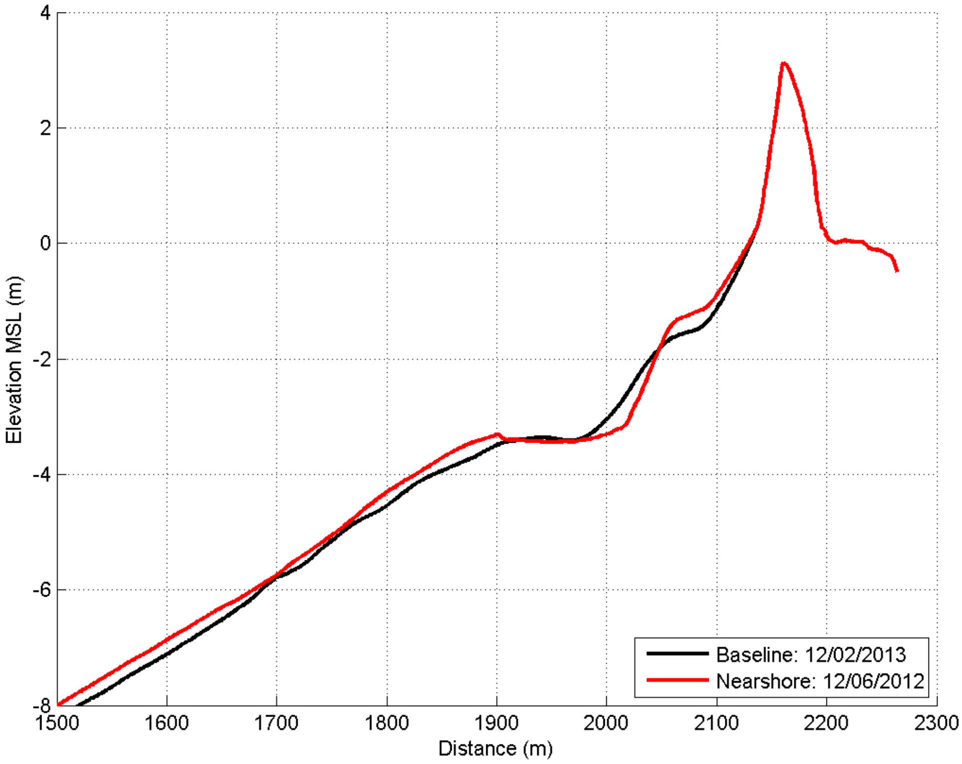

Figure 10 – Profiles with different nearshore morphologies. The subaerial section was measured after the overwash episode, while the nearshore section was measured in February 2013 (labelled Baseline, with the date closest to the overwash episode). The nearshore section was also measured in other occasions, with profile Nearshore displaying the June 2012 morphology.

5. HYDRODYNAMIC MODELLING

5.1. MODEL SET-UP: Barreta baseline overwash model

This study uses the one-dimensional approach of XBeach model developed by Roelvink et al. (2009). XBeach is a process-based hydrodynamic and morphodynamic model developed to assess the natural coastal response to time-varying storm and hurricane conditions. In this study the model was run in non-hydrostatic (wave-resolving) mode (Smit et al., 2012; McCall et al., 2014), including groundwater processes (McCall et al., 2012; McCall et al., 2014), but without the computation of morphological changes. Model setup consisted of three stages: definition of boundary forcing conditions, generation of the model grid and parametric adjustments. The boundary forcing conditions were definedusing field data, when available, or from modelled outputs. Variables used as boundary conditions include: barrier profile (Figures 9 and 10), modelled wave spectra at depths of MSL-12 m, -15 m and -17 m (details in section 3.1) (Figure 5B), ocean and lagoon water levels (Figure 5A), and D_{50} (Table 1), whilst other non-measured parameters were kept at their default values (e.g., bed friction). The hydraulic conductivity (K) was computed with Hazen's equation (Table 1), using measured D_{10}. The generated grid is non-equidistant, with a minimum grid size of 0.1 m onshore and a maximum grid size of 3 m offshore, observing the limiting condition of a minimum of 50 points per wavelength (Table 1).

Table 1 – Input parameters for XBeach model.

Parameter	
Minimum grid size (m)	0.1
Maximum grid size (m)	3
Minimum points per wavelength	50
Offshore boundary	Z = -15 m
Duration (s)	2340 ; including 600 s spin-up
Output timestep (s)	0.25
D_{50} (m)	0.00061
K (ms^{-1})	0.0015

Validation of the model is achieved by comparison of observed and modelled wave runup and overwash statistics. While no observed nearshore spectral wave data were available for a quantitative validation of the nearshore wave height, Figure 6 does qualitatively illustrate the changes in the modelled wave spectra across the nearshore profile during the overwash episode. Wave energy decreased as waves propagated into the nearshore, with the most significant transformations occurring between depths of MSL -4 m and the shoreline. As depth decreases and waves propagate landward of the nearshore bar there was an increase in wave energy on the infra-gravity band and the widening of the spectra, particularly noticeable for narrow offshore spectra conditions (e.g., Figure 6 A and 6D).

Further XBeach setup adjustments were carried out on the offshore boundary, spin-up duration and number of replicates. The offshore extent and depth at the offshore boundary of the XBeach model was decided by balancing two opposite criteria: (i) the boundary should be located in relatively deep water to correctly account for infragravity wave energy associated with long-period incident-band waves; and (ii) it should be located in water shallow enough to account for most of wave refraction and to minimize dispersion errors related to the numerical scheme of the model. Considering the wave conditions measured during the overwash episode and a ratio between wave group velocity and phase velocity < 0.85 (Deltares, 2014), a boundary at depths bellow MSL-17 m would be preferable. However, as waves at this depth were not yet shore-normal (12^{o} - 26^{o} relative to shore-normal) and refraction cannot be accounted for in a 1D model, as a compromise, the offshore boundary was set in an intermediate location, at MSL -15 m. For XBeach, the offshore boundary was set at x = 0 m and z = - 15 m (Table 1), and the domain, represented in Figure 4, has a cross-shore extension of 1730 m. XBeach in non-hydrostatic mode is a phase-resolving model; therefore, at the start of each run waves propagating across the nearshore do not reach the barrier, and the groundwater surface needs time to adjust. Runs were made with an initial time (the ‘spin-up’) of 10, 20 and 30 minutes durations. It was concluded that a spin-up of 10 minutes provided good results whilst maintaining a reasonable computational effort.

Since the XBeach model simulates hydrodynamics based on a random realisation of the imposed wave-spectra, which are statistical quantities obtained over 30-minutes, model results may vary between simulations with the same statistical boundary conditions, but different random realisations of the wave field. Figure 11 shows the variation in the average number of overwash events with an increase in the number of replicates. Replicates in this context are model runs of the nine 30-minutes time-steps, with exactly the same input conditions (e.g., grain-size, grid size, tide elevation, spectra parameters). For each replicate, an overall number of overwash events was obtained (270 minutes duration of the overwash episode). A power analysis was performed to estimate the number of replicates (sample size) needed to allow accurate and reliable statistical evaluation. In this context, power analysis serves to estimate the number of modelling replicates needed to have a good chance of detecting overwash differences between different tests that are not due to differences in random realisations of the wave field. To conduct the power analysis, it was necessary to set a number of variables: mean and standard deviation of number of overwash events, effect size, and power. The effect size is the minimum deviation that needs to be detected, while power is the probability of distinguishing a minimum effect. An effect size of 10% and a power of 95% were decided based on the literature (e.g. McDonald, 2014), and assured a very high chance of observing an effect that is real. A mean number of 160 overwash events and a standard deviation of 10 were used (Figure 11) for power computation. The obtained number of replicates was 6. The overwash episode was divided into 9 time steps of 30 minutes (with 10 minutes spin-up), from 08:30 to 12:30. The output time-step was set at 4 Hz, matching the sampling grid of the instruments.

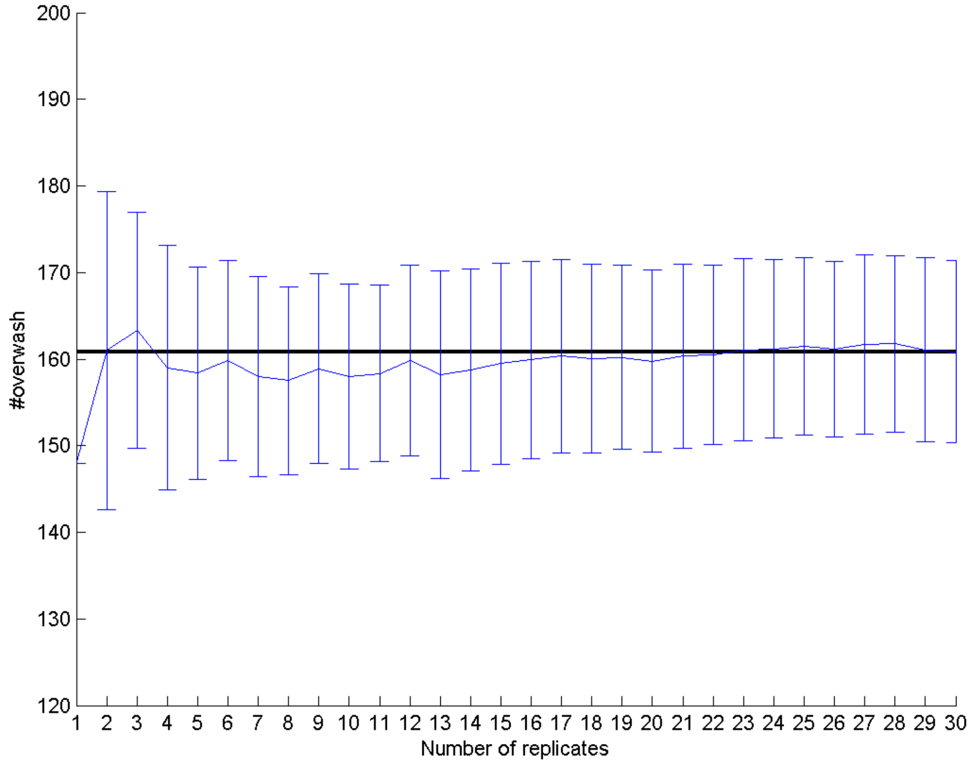

Figure 11 – Average and standard deviation of overwash number of events for the entire episode considering an increasing number of replicates. The coarser black line is the overwash number of events after 30 replicates (161 events).

5.2. BASELINE MODEL PERFORMANCE

The performance and evaluation of model usefulness as a predictive tool was assessed using standard metrics of performance, particularly bias (eq. 1), root-mean-square error (RMSE, eq. 2), and scatter index (SCI, eq. 3), as described in

McCall et al. (2014). The model overwash statistics for each 30-minute period i ($x_{i,modelled}$), were compared against overwash statistics computed from field data for the same duration ($x_{i,measured}$). The mean error describes the potential bias as follows:

$$\text{Bias}(x) = \frac{1}{N}\sum_{i=1}^{N}(x_{i,modelled} - x_{i,measured}) \quad (1)$$

Where N is the number of time-steps (9 for this particular case). The RMSE measures the difference between values predicted by a model and the values actually observed from the environment that is being modelled, and is defined as follows:

$$\text{RMSE}\ (x) = \sqrt{\frac{1}{N}\sum_{i=1}^{N}(x_{i,modelled} - x_{i,measured})^2} \quad (2)$$

SCI is a relative measure of the scatter between model and data as follows:

$$\text{SCI}\ (x) = \frac{\text{RMSE}(x)}{\max\left(\frac{1}{N}\sum_{i=1}^{N} x_{i,measured};\ \sqrt{\frac{1}{N}\sum_{i=1}^{N} x_{i,measured}^2}\right)} \quad (3)$$

The error is normalized with the maximum RMSE of data and the absolute value of the data mean to avoid anomalous results for data with small mean and large variability. Bias, RMSE and SCI closest to zero represent better model performances.

The model performance metrics are presented in Table 2. Results indicate that the model overestimates the number of overwash events; for all time-steps an average of 5 additional overwash events are produced by the model, which represents an overestimation of approximately 25 %. The baseline model performance changes throughout the event; during the rising tide the baseline model under- or over-predicts by only 2-4 events, while during the falling tide the baseline model over-predicts overwash by 4-14 events.

Table 2 – Summary of performance metrics of baseline model according to average number, depth and velocity of overwash events. Values are averages for all time-steps.

Parameter	Model performance		
	Bias	RMSE	SCI
Number of overwash events	5	7	0.27
Peak overwash depth (m)	0.02	0.02	0.30
Peak overwash velocity (ms^{-1})	0.43	0.61	0.28

Overwash depth and velocity are also overestimated by about 20%; however, these values are very small (0.02 m and 0.4 ms^{-1}) and within the error margin of the measurements under the demanding fieldwork conditions. The SCI for the number, depth and velocity of overwash events is consistently low to moderate (c. 0.3).

The comparison between the fieldwork runup statistics and the modelled runup statistics is also an indicator of the model performance. The average difference between the field R_{sig} and the model R_{sig} each 10 minutes is 0.2 m, with the model overestimating conditions measured in the field. Because overwash flows are so shallow, a 0.2-m difference in significant runup represents an increase of 25% of overwash events over the crest, which may be due to overestimation of offshore water level or wave swash computations.

5.3. BASELINE MODEL VERIFICATION

In order to verify that the Barreta baseline overwash model consistently provides reasonable predictions of overwash, the model was applied to other situations when overwash was measured in the same profile, at Barreta Island, during the period referred previously (June 2012 to April 2013). Field surveys, including topography and bathymetry, were undertaken before and after each of six overwash episodes, although no instrumentation was deployed on the barrier and thus there were no measurements of runup or overwash hydrodynamics. For the post-overwash episode surveys, the maximum overwash intrusion on the barrier island top was surveyed in detail with RTK-DGPS (for further details about this dataset refer Matias et al., 2014). Measured offshore waves for the overwash episodes were used to force nearshore wave propagation as described for the calibration fieldwork (section 3.1).

The six post-overwash topo-bathymetric surveys, named for simplicity as "Episode 1" to "Episode 6" characteristics can be found in Table 3. Episode 1 to Episode 6 characteristics (morphology, waves, maximum tide level) were used as inputs to the calibrated baseline model, while other parameters remained unaltered. For each modelled overwash episode, the location of the maximum water intrusion on top of the barrier was extracted and compared with fieldwork (Figure 12).

Table 3 – Conditions of the six overwash episodes verification cases

	Date	Hs	Tp	Tide
Episode 1	02/10/2012	0.73	9.1	1.35
Episode 2	31/10/2012	2.15	9.4	1.31
Episode 3	19/11/2012	2.01	8.6	1.92
Episode 4	31/01/2013	1.02	12.5	1.36
Episode 5	13/02/2013	0.79	9.4	1.51
Episode 6	13/03/2013	1.40	9.41	1.80

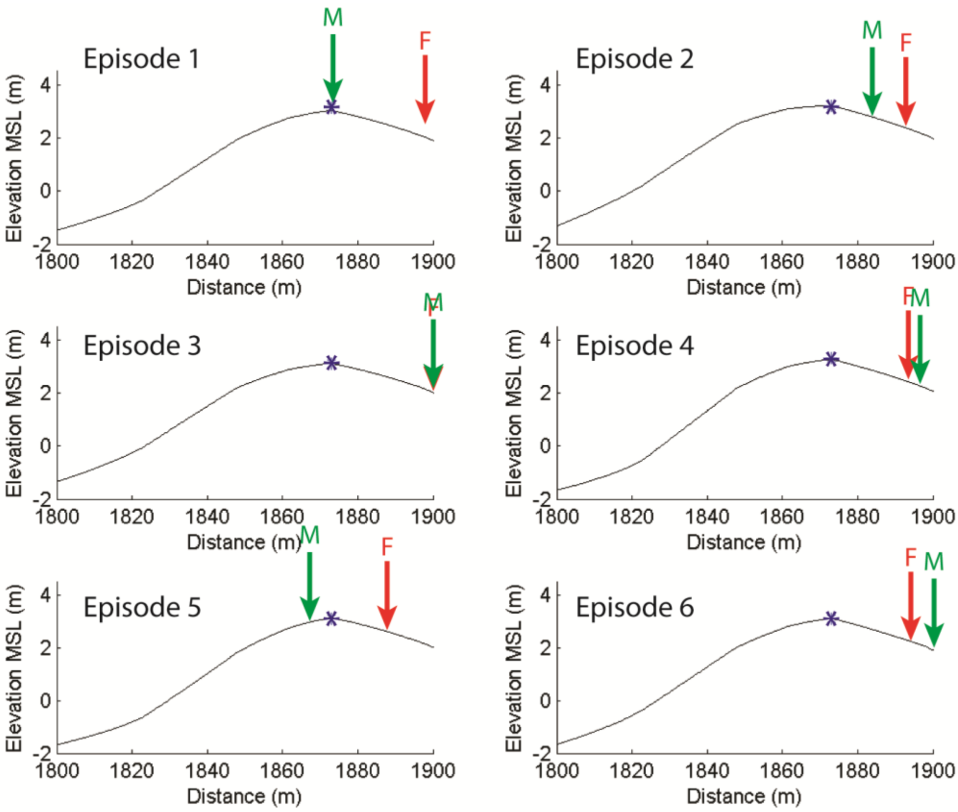

M - model max intrusion F - field max intrusion * barrier crest location

Figure 12 – Maximum overwash water intrusion over the barrier crest obtained during fieldwork measurements and after modelling results.

Results show that the modelled and measured maximum water intrusion have relatively good agreement, although not always coincident (average horizontal difference = 8.6 m and average vertical difference = 0.2 m). Minimum difference in overwash water intrusion across the barrier is close to zero (Episode 4, Figure 12) and maximum difference was observed for Episode 1, where fieldwork measurements show a maximum swash excursion of 56.5 m from the average water line position, thus causing significant overwash and the model estimated a swash excursion of 31.5 m. During Episode 5, the model failed to predict overwash occurrence, although by a small amount (Figure 12). This result is somewhat unexpected since the results of the calibration have shown that the model over-predicts overwash by 20 to 25%. Limitations in correctly identifying the line of maximum intrusion of a specific episode, in an area where overwash occurs frequently, may be one cause of this mismatch, alongside errors in model boundary conditions such as the (dynamic) submarine and subaerial barrier profile (see e.g., Section 6.2). When possible, fieldwork was undertaken only a few hours after overwash, when the overwash debris line was coincident with a wet/dry sand line. However, in case of Episode 1 such an early survey was unfeasible due to technical constraints and it is possible that the marked debris line (marked F in Figure 12) may corresponded to a previous overwash episode.

Overall, the Barreta baseline overwash model performs fairly well in predicting hydrodynamics in the study area, because the BIAS, RMSE and SCI are relatively small, and the verification episodes are also generally well simulated.

6. MODELLING ANALYSIS

The Barreta baseline overwash model was further explored to analyse the relative importance of several factors in overwash occurrence, namely: (1) hydrodynamic parameters, particularly waves and lagoon water levels; and (2) nearshore morphological configurations of the barrier and barrier grain-size. To evaluate the contribution of these factors, the Barreta baseline overwash model was changed in only one parameter at a time, keeping the remaining unaltered. Each modified model was also replicated six times (see section 5.1) and ensemble-mean results are presented. The output variables (runup, number of overwash events, overwash depth, velocity and discharge) were compared with the baseline model, aiming to understand their relative importance in overwash processes.

6.1. HYDRODYNAMIC PARAMETERS

The wave conditions used to setup and verify the Barreta overwash model have an annual probability of occurrence of about 50%, for waves from W and SW. (according to data described in Costa et al., 2001). To observe how much overwash hydrodynamic parameters change under more extreme (less frequent) conditions, a set of simulations named "waveplus" were defined, where all parameters remained unaltered, except the waves (Table 4). According to Costa et al. (2001), the joint probability of H_s = 1 – 3 m and T_p= 7 – 11 s is 8.5%, whilst the joint probability of H_s=3 - 5 m and T_p=11 - 15 s is only 0.1%. Nine conditions were modelled and replicated six times, progressing from the baseline model to low-probability conditions with H_s of 4 m and T_p of 15 s (waveplus 9). Since this test aimed to observe increased overwash magnitudes, only peak high-tide water levels (z= 0.88 m MSL) were considered. During these simulations, the barrier remained in the overwash regime and not in the inundation regime (as defined by Sallenger, 2000) and the barrier crest was not permanently submerged.

Table 4 – Significant wave heights and peak periods for the "waveplus" simulations.

	Hs	Tp	Probability (%)*
Baseline	1.68	11.1	
waveplus 1	2	11	8.5
waveplus 2	3	11	
waveplus 3	2	12	
waveplus 4	3	12	5.3
waveplus 5	3	13	
waveplus 6	3	14	0.1

waveplus 7	3	15
waveplus 8	4	14
waveplus 9	4	15

*According to data from Costa et al. (2001).

For the most extreme conditions simulated, overwash maximum depth can reach up to 1 m (Figure 13A), which is only comparable to the field dataset of Fisher and Stauble (1977) that reported overwash induced by Hurricane Belle on Assateague Island (USA). Maximum overwash velocities reach 9 ms^{-1}, which are very high compared to typical measurements in the field (around 2 ms^{-1}, Matias and Masselink, 2017) and maximum leading edge velocities measured in the field (6 ms^{-1} this study and fieldwork of Almeida et al., 2017), and comparable to the maximum velocities measured in the laboratory (10 ms^{-1}; Matias et al., 2014). Average overwash depth and velocity under extreme wave conditions does not increase as much as maximum overwash depth and velocity because the number of smaller overwash events also increases. The percentage of time when seawater is overtopping the crest is high, particularly for the bigger waves (about 58% of time, Figure 13). The results show that for each wave height case that was modelled, there was only a small increase in the number of overwash events with longer peak wave periods (Figure 13).

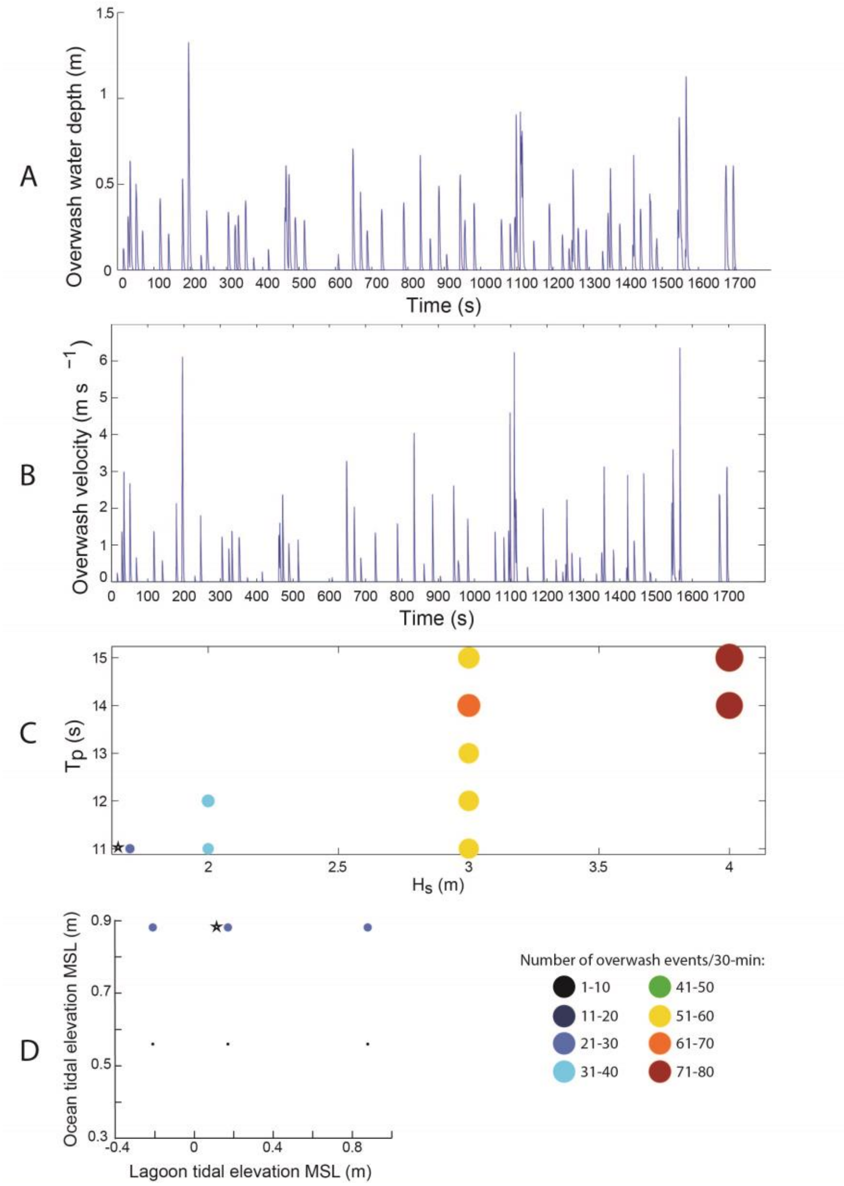

Figure 13 – Time-series of overwash depth (A) and overwash velocity (B) for one of the replicates of series waveplus, run 9 ($H_s = 4$ m; Tp = 15 s). C. Comparison between different waveplus models with varying Hs and Tp. D. Comparison between different lagoon water level tests. The circle size is proportional to the number of overwash events. The stars identify the baseline model.

To test the importance of lagoon levels in overwash occurrence, the model was run with the maximum ocean and lagoon water level difference for the fieldwork campaign. The baseline model hydraulic gradient was always negative (between -0.0054 and -0.0132, towards the lagoon), because the lagoon levels were consistently lower. To test other situations, high, mean and low lagoon water levels cases were implemented (z= 0.88, 0.17 and -0.21m MSL), with two ocean water levels (z= 0.88 and 0.56 m MSL). These changes generated model simulations with the highest hydraulic gradient (0.006) for the high lagoon model and a minimum hydraulic gradient (-0.01) for the lagoon low-tide model, during oceanic high-tide. Even if the lagoon water level could be lowered, the hydraulic gradients would not change significantly because of the backbarrier morphology (Figure 2A). As the water level reaches the backbarrier low-tide flat, a small change in elevation implies a great increase in horizontal distance, thus lowering the gradient. The results of the high lagoon, low lagoon and the baseline models present small average variations (Figure 13C). The average variation in overwash number between the lagoon models was only 1 event, for both oceanic tidal elevations, which is not statistically significant. Note however that greater differences in morphodynamic response of the back barrier may occur, particularly during larger overwash events, as a result of changing hydraulic gradients between the ocean and lagoon (e.g., Suter et al., 1982; Donnely et al., 2006; McCall et al., 2010).

6.2. BARRIER PARAMETERS

The nearshore morphology is known to change significantly in the study area (e.g. Vila-Concejo et al., 2006), as a consequence of the migration of swash bars from the updrift Ancão Inlet. Several nearshore morphological configurations of the study area were available (data from Matias et al., 2014, also mentioned in section 5.3, Figure 10) and the one that deviates most from the configuration during the December 2013 overwash episode was selected for modelling overwash. The survey in June 2012 showed a significantly higher nearshore bar crest in comparison to the configuration used for the baseline model (Figure 10). The new bathymetric grid was built with the same resolution and dimensions of the baseline model, and the same oceanographic forcing was superimposed, which implied new SWAN runs over the new bathymetric grid.

Significant differences are observed between the baseline model and the model with a modified nearshore bathymetry (termed “nearshore model”; Figure 14). There is a noticeable reduction in the number of overwash events with the nearshore model compared to the baseline model, from 160 to 105 events, particularly evident during high-tide when the reduction reaches more than 40%.

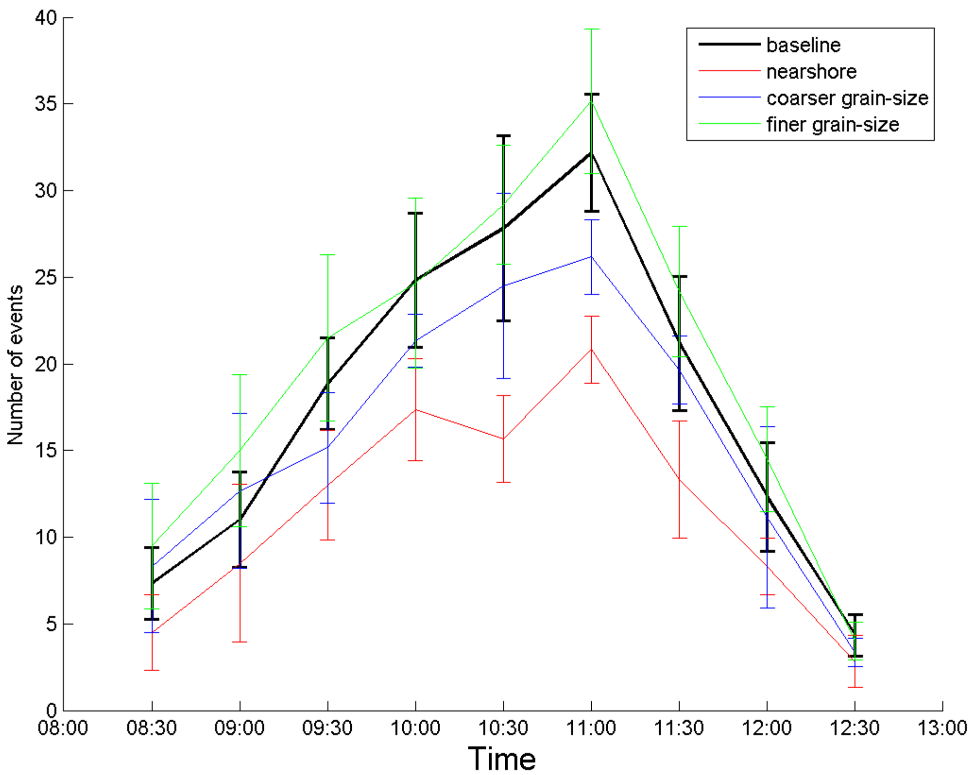

Figure 14 – Average and standard deviation of overwash number of events for each time-step of the baseline model, nearshore model, coarser and finer grain-size models.

The average overwash depth, velocity and discharge are also different under the two configurations, but the reduction is relatively small (-2 mm average depth, -0.06 ms^{-1} overwash velocity and -0.01 $m^3m^{-1}s^{-1}$; Figure 15). Overall, overwash water discharge during the entire episode for the baseline model was 45 m^3m^{-1} (summing the discharges of 160 events) while for the nearshore model this was 27 m^3m^{-1} (total of the 105 events) which corresponds to a 40% reduction, mostly due to decrease in number of overwash events. The runup statistics (not shown here) evidence a reduction in runup on the nearshore model (R_{sig} decreased 0.22 m in relation to baseline model). Average R_{sig} of the nearshore model is, however, closer to fieldwork than the baseline model because it is truncated by the barrier crest elevation.

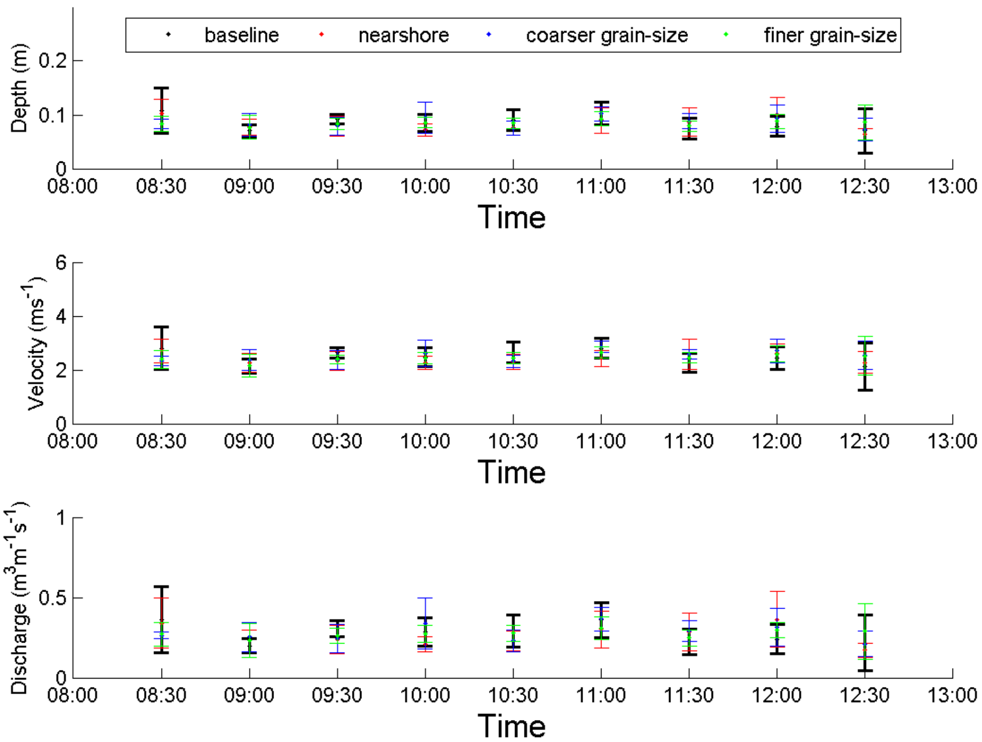

Figure 15 – Average depth and velocity of overwash events during each time-step of baseline model, nearshore model, coarser and finer grain-size models. Average number of events for each time-step of the baseline model and the different grain-size models.

Previous studies in Barreta Island (Matias et al., 2009) indicated variability of barrier grain-size, both on the beach face and in the barrier washovers. This information was used to obtain a measure of the likely grain-size variability and hence set the finer and coarser grain-size models. The finer grain-size model was set with D_{50} = 0.47 mm, which implied a change of K to 0.001 m s^{-1}, whilst the coarser grain-size model was set with D_{50} = 0.89 mm and K=0.0039 m s^{-1} (Table 5).

Table 5 – Grain-size parameters (D_{50} and D_{10}) and hydraulic conductivity (K).

	D_{50} (m)	D_{10} (m)	K (m/s)
Fieldwork	0.00061	0.00039	0.0015
Coarser*	0.00089	0.00063	0.0039
Average*	0.00065	0.00041	0.0017
Finer*	0.00047	0.00032	0.0010

*According to data from Matias et al. (2009).

The comparison between the baseline model and the finer and coarser grain-size models showed that the finer grain-size model was the one producing more overwash, while the coarse grain-size model led to a decrease in overwash number (Figure 14), probably due to enhanced infiltration. The change in overwash events was significant, from 160 in the baseline model to 178 in the finer model and 142 in the coarser model. Again, the changes were particularly evident in the number of overwash events comparing to the other hydrodynamic variables (depth and velocity changes were always smaller than 1 mm and 0.03 ms^{-1}, respectively; Figure 15). Overall discharges reduced 8% in the coarser and increased 7% in the finer grain-size models in relation to the baseline model. R_{sig} of coarser grain-size model decreased 0.03 m in relation to baseline, while average R_{sig} of finer grain-size model increased in 0.01 m.

7. DISCUSSION

Overall, morphological changes and hydrodynamic parameters observed during the 12th of December 2013 overwash episode in Barreta Island compare well with recent field and laboratory measurements of overwash dynamics. Small morphological changes, characterized by sediment erosion across the subaerial beach, but only partially deposited on the barrier top, suggest offshore sediment transport to the sub-tidal section of the profile of at least part of the eroded sediment. Similar morphological evolution was observed in recent high-resolution 2D laser scanner measurements of overwash by Almeida et al. (2017). In terms of hydrodynamic parameters, the most common overwash flow during the overwash episode was very shallow (mean depth of 0.067 m) and relatively fast, with peak velocities in the range 1 – 3 ms^{-1}. Such supercritical flows agree with typical fieldwork and laboratory measurements that can be found in Matias and Masselink (2017).

Because field measurements are scarce and difficult to obtain, and laboratory datasets may have scale and applicability limitations, reliable numerical models simulating overwash are valuable to complement field data (e.g. Matias et al., 2017), While there were limitations in data collection, given the energetic nature of overwash conditions, the field measurements obtained in Barreta Island complement the scarce datasets that are available to test numerical models that simulate overwash (Matias et al., 2017). This innovative field dataset was complemented with published data from overwash on Barreta Island and used to setup a baseline model of overwash hydrodynamics using XBeach in non-hydrostatic mode, expanding the evidence base of the model's ability to reproduce hydrodynamic processes during overwash at field-scale. The baseline model replicates have a maximum of 18% variation in overwash number, and 40%, 27% and 100% maximum variation in average overwash depth, velocity and discharge for 30-minute simulations, respectively. Such large variability between replicates (standard deviation on number of overwash evets= 10-17) clearly evidence the need for replication when using wave-resolving models to compute representative statistical properties. Moreover, it demonstrates how field/buoy measurements condensed in wave spectra, instead of the actual sequence of surface wave elevations, can represent slightly different conditions and thus translate into variability and uncertainty in simulation of coastal processes.

The baseline model performance metrics were assessed by comparison with fieldwork using established error metrics, namely bias, RMSE and SCI (McCall et al., 2014). The results indicate that the baseline model has variable skills over the duration of the overwash episode, performing better during the rising tide than during the falling tide. The baseline model has a positive bias, therefore overestimates the number of overwash events, and an overall RMSE = 7 and SCI = 0.27. These differences between predictions and observations may be related to several factors, mainly related to uncertainty in the field observations. Morphologic changes occurring during overwash in the submerged, non-monitored part of the beach profile can influence subsequent overwash hydrodynamics, as nearshore morphology has been shown to influence the frequency and intensity of overwash (Ritchie and Penland, 1988; Matias et al., 2014. Moreover, the baseline model was set with the most recent bathymetry in the area, measured in February 2013, 10 months before the overwash fieldwork. Additionally, there is a lack of measured wave data in the nearshore and swash zones, as only offshore wave parameters were obtained from observations. Nearshore wave transformation was simulated with the model SWAN, which is a well-established model for nearshore wave propagation, but no quantitative validation can be performed with field data as instruments in stations ST1 and ST3 collapsed or failed during the overwash episode. However, the qualitative analysis of nearshore wave spectra transformation (Figure 6) suggests that the results for wave modelling are within the expected range of changes for shallow waves as they propagate across nearshore bars. Difference in model skill for the rising and falling tide can be explained by the small but positive changes in barrier crest, which built up during the rising tide (~5 cm, Figure 9), and small changes in the tide and surge along the coast, meaning the imposed ocean water level is less accurate in the falling tide than the rising tide.

While recognizing the natural limitations in fieldwork measurements during such energetic events, as well as various possible sources of error and uncertainties in model implementation, it was considered that the baseline model provided a reasonable agreement with field data, which is substantiated by the performance metrics and by the six additional verification cases. Encouraging results of XBeach implementation for overwash investigation were also obtained by McCall et al. (2010) on a sandy beach, Almeida et al. (2017) on a gravel beach and Masselink et al. (2014) in laboratory experiments. The fieldwork case, i.e., the baseline model was set without tuning parameters and relying on default XBeach parameterizations, implemented solely based in data from previous fieldwork (e.g. bathymetry), local data published in the literature (e.g., offshore bed grain-size), empirical relations (e.g. between grain-size and hydraulic conductivity) and wave modelling (SWAN model). This methodology is not, however, free of intrinsic and extrinsic errors, since there is significant inter- and intra-annual variability of bathymetry, topography and grain-size (e.g., Vila-Concejo et al., 2002; Matias et al., 2004) and empirical relations used in morphodynamic and wave modelling are also approximations to real physical conditions.

To evaluate the contribution of the several factors locally influencing overwash hydrodynamics based on modelling results, several case models were simulated with different ocean conditions and barrier variables, all within the natural variability of the area. The probability of joint distribution of wave height and period published in the literature was used to simulate overwash under more energetic and infrequent oceanographic conditions (the “waveplus” models). Results suggest that modelled overwash number is more sensitive to changes in the wave height than variations in wave period, which may be related to the limited range of wave heights and periods used for this simulation. For instance, laboratory measurements made by Matias et al. (2012) showed a significant increase of overwash frequency when the wave period was manipulated on controlled flume experiments. However, due to its NW-SE orientation (Figure 1), Barreta Island is not exposed to local sea conditions, which occur under SE winds and typical wave periods of 4-6 s, and only to SW swell waves trigger overwash events in this area. Therefore, overwash occurrence under the combination of high waves with shorter periods is not registered and hence not included in the current analysis.

Results show that fieldwork conditions, more frequent and within acceptable safety and logistic requirements, were relatively mild compared with the possible overwash magnitude with higher and longer period waves (Figure 13). According to modelling results, oceanographic conditions with a probability of about 0.1 %, can induce overwash episodes 3-4 times more intense. The low frequency of these events and fieldwork safety restrictions under these extreme conditions limits the acquisition of field measurements for the conditions when modelled overwash velocities peak over 8 ms^{-1}. Even under relatively shallow flows, less than 1 m depth in the waveplus 9 case, these supercritical flows may discharge more 7 $m^3m^{-1}s^{-1}$, which are beyond acceptable safety levels for people and instrument deployment on the coast. This means that future application of the baseline model to predict overwash occurrence and hydrodynamics will be more sensitive to uncertainties in the predictions of significant wave height, and less sensitive to uncertainties in predictions of peak wave period, considering the range of observed values the study area.

The ocean tidal level is a fundamental factor in the occurrence of overwash, and it is included in all runup equations, overwash empirical relations and numerical model predictions. However, the role of the lagoon tidal level in overwash hydrodynamics was not established in this area. The modelled cases "lagoon high" and "lagoon low" were set to cover positive and negative hydraulic gradients that did not occur during fieldwork (and are impossible to measure in the study area due to its present configuration, distance to the inlet, backbarrier tidal flat morphology, etc.), but that could produce relevant contrasting scenarios that enhance the insights that can be obtained from model simulations. Assuming that the model reproduces correctly the groundwater flows, results from this study suggest that the lagoon water elevation has little effect (less than 1%) on overwash hydrodynamics (Figure 13). Almeida et al. (2017) implementation of Xbeach model on a gravel barrier also found that groundwater gradients do not produce a significant difference in modelled overwash discharges. This implies that in a data scarce situation, efforts to obtain accurate predictions or observations of lagoon tidal level are not as relevant as other parameters to enhance model performance.

The contribution of barrier morphological characteristics to overwash hydrodynamics was also evaluated in this study. Barrier topography, particularly barrier crest elevation but also beach slope, are critical factors that are included in all current methods to predict overwash. For example, the role of beach morphology was found to be crucial in modelling wave overtopping with XBeach by Phillips et al. (2017), in an area of North Wales, U.K., where exposure to coastal flooding hazards are significant. In our study, the nearshore bathymetry was also evaluated by setting the "nearshore model", which was identical to the baseline model except for the bathymetry that was changed to the surveyed morphology that differs mostly from the baseline configuration and is characterized by a more pronounced nearshore bar. Results indicate an average difference of about 30% of overwash events, with the nearshore model inhibiting overwash (Figure 14). Based on these results, it was considered that the nearshore bar, particularly wave transformation and dissipation that occurs as waves propagate over the nearshore bar, is an important factor in overwash hydrodynamics. Nearshore morphological variability in this area is significant, given the detachment and longshore migration of swash bars from the updrift Ancão Inlet, and therefore accurate and updated bathymetry is paramount for model performance and accuracy.

Although the main sedimentary source to the study area is relatively constant (longshore drift and inlet associated dynamics), some sand grain-size variability has been observed in the area (Table 5; Matias et al., 2009). The impact on model results arising from realistic grain-size changes was tested by running the "coarser" and “finer” grain-size models. The cases simulated are all within the same grain-size class, with a minimal distinction between medium and coarse sand. On average the coarser grain-size model promoted less overwash (-11% overwash events number and -8% discharge), than the baseline model. An intensification of overwash was recorded with the finer grain-size model. This means that there may be small to moderate overwash hydrodynamic changes in the study area induced solely by a relatively limited natural grain-size variability. Previous work in a longshore variable setting showed that 2D modelling can significantly increase model accuracy in case of complex bathymetric configurations (e.g. Lerma et al., 2017).

8. CONCLUSION

Data from an overwash episode in Barreta Island (Portugal) are presented in this study. The overwash episode occurred during mid-tide to high-tide (maximum oceanic tidal elevation of 0.9 m above MSL), with bimodal waves that resulted from the combination of swell waves with variable periods and heights. During this moderate energy event, overwash was not prevalent along most of the Ria Formosa barrier islands as wave runup was consistently lower than dune crest elevation. However, in the fieldwork study site (a low-lying barrier stretch) experienced more than 100 overwash events. Fieldwork observations, modelled nearshore wave spectra and published data on overwash dynamics in Barreta Island were used to setup XBeach in non-hydrostatic mode and develop a baseline model of overwash hydrodynamics. The baseline model was verified against field data, demonstrating a good agreement according to standard metrics for model performance (bias, RMSE and SCI), with maximum errors of 20% to 25% error for different overwash variables. Overall, there was an 83% agreement between observed and predicted overwash episodes.

Using recent observations of hydrodynamic forcing and morphological changes for the area, a set of realistic scenarios was modelled to test the contribution of different variables for overwash hydrodynamics. Results indicate that the wave height is the factor that influenced model results the most (up to 400%), followed by the nearshore bathymetry (up to 30%) and to a lesser extend grain-size (up to 11%). The relatively small impact of some parameters considered crucial on runup and overwash, such as wave period, is due to the natural small range of realistic wave periods that are observed during storms in the study area. This implies that confidence in model predictions is mainly dependent on the quality of wave height and water level boundary conditions imposed on the model, as well as up-to-date barrier parameters, primarily the nearshore bathymetry and barrier configuration and also the grain-size.

ACKNOWLEDGEMENTS

This study was supported by RUSH project, PTDC/CTE-GIX/116814/2010 and EVREST project, PTDC/MAR-EST/1031/2014, financed by FCT, Portugal. A. Matias and A. Pacheco were supported by Investigator Programme, IF/00354/2012 and IF/00286/2014, respectively, financed by FCT, Portugal. A.R. Carrasco was supported by SFRH/BPD/88485/2012. Carlos Loureiro is funded by the EU H2020 MSCA research project NEARControl (Grant Agreement No 661342). T. Plomaritis was funded by the EU FP7 research project RISC-KIT (ref. RISC-KIT-GA-2013-

603458). R. McCall was funded by the EU FP7 RISC-KIT project and Deltares Strategic Research in the "Hydro-and morphodynamics during extreme events" program (1230002). Umberto Andriolo was supported by the EARTHSYSTEM Doctorate Programme led by Institute Dom Luiz Associate Laboratory at the University of Lisbon (SFRH/BD/52558/2014).

REFERENCES

Almeida, L.P., Masselink, G., McCall, R., Russell, P., 2017. Storm overwash of a gravel barrier: field measurements and XBeach-G modelling. Coastal Engineering, 120, 22-35.

Andriolo U, Almeida LP, Almar R. 2018. Coupling terrestrial LiDAR and video imagery to perform 3D intertidal beach topography, Coastal Engineering, 140, 232-239.

Atkinson, A. L., Power, H. E., Moura, T., Hammond, T., Callaghan, D. P., Baldock, T. E., 2017. Assessment of runup predictions by empirical models on non-truncated beaches on the south-east Australian coast. Coastal Engineering, 119, 15-31.

Baldock, T.E., Hughes, M.G., Day, K., Louys, J., 2005. Swash overtopping and sediment overwash on a truncated beach. Coastal Engineering, 52, 633-645.

Baumann, J., Chaumillon, E., Bertin, X., Schneider, J.-L., Guillot, B., Schmutz, M., 2017. Importance of infragravity waves for the generation of washover deposits. Marine Geology, 391, 20-35.

Blenkinsopp, C., Matias, A., Howe, D., Castelle, B., Marieu, V., Turner, I., 2016. Wave runup and overwash on a prototype-scale sand barrier. Coastal Engineering, 113, 88-103.

Blott, S.J. and Pye, K., 2001. GRADISTAT: a grain size distribution and statistics package for the analysis of unconsolidated sediments. Earth Surface Processes and Landforms, 26, 1237-1248.

Booij, N., Ris, R.C., Holthuijsen, L.H., 1999. A third-generation wave model for coastal regions: 1. Model description and validation. Journal of Geophysical Research, C4, 104, 7649-7666.

Bouguet, J.Y., 2007. Camera Calibration Toolbox for Matlab. Available in: http://www.vision.caltech.edu/bouguetj/calibdoc/.

Bray, T.F. and Carter, C. H. 1992. Physical processes and sedimentary record of a modern, transgressive, lacustrine barrier island. Marine Geology, 105, 155-168.

Cleary, W. J., McLeod, M. A., Rauscher, M. A., Johnston, M. K., Riggs, S. R., 2001. Beach nourishment on hurricane impacted barriers in Southeastern North Carolina, USA: Targeting shoreface and tidal inlets sand resources. Journal of Coastal Research SI 34, 232-255.

Costa, M., Silva, R., Vitorino, J., 2001. Contribuição para o estudo do clima de agitação marítima na costa portuguesa. Proceedings of 2as Jornadas Portuguesas de Engenharia Costeira e Portuária, International Navigation Association PIANC, Sines, Portugal (in Portuguese).

Deltares, 2014. XBEACH-G – Storm impact model for gravel beaches: user manual, at: https://oss.deltares.nl/web/xbeach/xbeach-og

De Vet, P.L.M., R.T. McCall, J.P. Den Bieman, M.J.F. Stive and M. Van Ormondt (2015). Modelling dune erosion, overwash and breaching at Fire Island (NY) during Hurricane Sandy. Proceedings of Coastal Sediments 2015, San Diego, USA, 11-15 May 2015.

Dolan, R. and Godfrey, P., 1973. Effects of Hurricane Ginger on the barrier islands of North Carolina. Geological Society of America Bulletin, 84, 1329-1334.

Donnelly, C., Kraus, N., Larson, M., 2006. State of knowledge on measurement and modeling of coastal overwash. Journal of Coastal Research, 22(4), 965–991.

Figlus, J., Kobayashi, N., Gralher, C., Iranzo, V., 2011. Wave overtopping and overwash of dunes. Journal of Waterway, Port, Coastal, and Ocean Engineering, 137, 26-33.

Fisher, J.S. and Stauble, D.K., 1977. Impact of Hurricane Belle on Assateague Island washover. Geology, 5 (12), 765-768.

FitzGerald, D.M., van Heteren, S., Montello, T.M., 1994. Shoreline processes and damage resulting from the Halloween Eve Storm of 1991 along the North and South shores of Massachusetts, USA. Journal of Coastal Research, 10, 113-132.

Hughes, M.G., Moseley, A.S., Baldock, T.E., 2010. Probability distributions for wave runup on beaches, Coastal Engineering, 57, 575–584.

Gama, C., Dias, J.A., Ferreira, Ó., Taborda, R., 1994. Analysis of storm surge in Portugal, between June 1986 and May 1988. Proceedings of the Second International Symposium on Coastal Zone Research-Management and Planning, EUROCOAST, Lisbon, Portugal, I, 381-387.

Leatherman, S.P., 1976. Quantification of overwash processes. Ph.D. Thesis, University of Virginia, USA.

Lerma, A.N., Pedreros, R., Robinet, A., Sénechal, N., 2017. Simulating wave setup and runup during storm conditions on a complex barred beach. Coastal Engineering, 123, 29-41.

Lindemer, C.A., Plant, N.G., Puleo, J.A., Thompson, D.M., Wamsley, T.V., 2010. Numerical simulation of a low-lying barrier island's morphological response to Hurricane Katrina. Coastal Engineering, 57, 985-995.

Martins, K., Blenkinsopp, C.E., Almar, R., Zang, J., 2017. The influence of swash-based reflection on surf zone hydrodynamics: a wave-by-wave approach. Coastal Engineering 122, 27-43.

Masselink, G., McCall, R., Poate, T., van Geer, P., 2014. Modelling storm response on gravel beaches using XBeach-G. Maritime Engineering, 167, 173-191.

Matias, A. and Masselink, G., 2017. Overwash processes: lessons from fieldwork and laboratory experiments. In: Coastal Storms: Processes and Impacts. (Ed.) Paolo Ciavola and Giovanni Coco, John Wiley & Sons Ltd., pp. 175-194.

Matias, A., Vila-Concejo, A., Ferreira, Ó., Morris, B., Dias, J.A., 2009. Sediment dynamics of barriers with frequent overwash. Journal of Coastal Research, 25 (3), 768–780.

Matias, A., Williams, J.J., Masselink, G., Ferreira, Ó. 2012. Overwash threshold for gravel barriers. Coastal Engineering, 63, 48-61.

Matias, A., Carrasco, A.R., Loureiro, C., Almeida, S., Ferreira, Ó., 2014. Nearshore and foreshore influence on overwash of a barrier Island. Journal of Coastal Research, SI 70, 675-680.

Matias, A., Masselink, G., Castelle, B., Blenkinsopp, C.E., Kroon, A. 2016. Measurements of morphodynamic and hydrodynamic overwash processes in a large-scale wave flume. Coastal Engineering, 113, 33-46.

McCall, R.T., de Vries, J.S.M., Plant, N.G., van Dongeren, A.R., Roelvink, J.A., Thompson, D.M., Reniers, A.J., 2010. Two-dimensional time dependent hurricane overwash and erosion modelling at Santa Rosa Island. Coastal Engineering, 57, 668-683.

McCall, R., Masselink, G., Roelvink, D., Russel, P., Davidson, M., Poate, T., 2012. Modelling overwash and infiltration on gravel barriers. Proceedings of the 33rd Conference on Coastal Engineering, Santander, Spain.

McCall, R.T., Masselink, G., Poate, T.G., Roelvink, J.A., Almeida, L.P., Davidson, M., Russell, P.E., 2014. Modelling storm hydrodynamics on gravel beaches with XBeach-G. Coastal Engineering, 91, 231-250.

McDonald, J.H. 2014. Handbook of Biological Statistics (3rd ed.). Sparky House Publishing, Baltimore, Maryland.

Muller, H.; van Rooijen, A.; Idier, D.; Pedreros, R., Rohmer, J., 2017. Assessing storm impact on a French coastal dune system using morphodynamic modeling. Journal of Coastal Research, 33(2), 254–272.

Pacheco, A., Ferreira, Ó., Carballo, R., Iglesias, G., 2014. Evaluation of the production of tidal stream energy in na inlet channel by coupling field data and numerical modelling. Energy, 71, 104-117.

Pawlowicz, R., Beardsley, B., Lentz, S., 2002. Classical tidal harmonic analysis including error estimates in MATLAB using T_TIDE. Computers & Geosciences, 28, 929-937.

Phillips, B.T., Brown, J.M., Bidlot, J.R., Plater, A.J., 2017. Role of beach morphology in wave overtopping hazard assessment. Journal of Marine Science and Engineering, 5, 1.

Popesso C., Pacheco A., Fontolan, G., Ferreira Ó., 2016. Evolution of a relocated inlet migrating naturally along an open coast. Journal of Coastal Research, SI (75), 233-237.

Pessanha, L.E. and Pires, H.O., 1981. Elementos sobre o clima de agitação marítima na costa sul do Algarve. Report of Instituto Nacional de Meteorologia e Geofísica. 66 p. (in Portuguese).

Ris, R.C., Holthuijsen, L.H., Booij, N., 1999. A third-generation wave model for coastal regions: 2. Verification. Journal of Geophysical Research, 104, C4, 7667-7681.

Ritchie, W. and Penland, S., 1988. Rapid dune changes associated with overwash processes on the deltaic coast of South Louisianna. Marine Geology, 81, 97-122.

Roelvink, D., Reniers, A., van Dongeren, A., de Vries, J., McCall, R., Lescinski, J., 2009. Modeling storm impacts on beaches, dunes and barrier islands. Coastal Engineering, 56, 1133–1152.

Roelvink, D., McCall, R., Mehvar, S., Nederhoff, K., Dastgheib, A., 2017. Improving predictions of swash dynamics in XBeach: The role of groupiness and incident-band runup. Coastal Engineering, 134, 103-123.

Rosa, F., Rufino, M., Ferreira, Ó., Matias, A., Brito, A.C., Gaspar, M., 2013. The influence of coastal processes on inner shelf sediment distribution: The Eastern Algarve Shelf (Southern Portugal). Geologica Acta, 11, 59-73.

Sallenger, A.H., 2000. Storm impact scale for barrier islands. Journal of Coastal Reseach, 16 (3), 890-895.

Salmon, J. and Holthuijsen, L., 2015. Modeling depth-induced wave breaking over complex coastal bathymetries. Coastal Engineering, 105, 21-35.

Smit, P., Stelling, G., Roelvink, J., Van Thiel de Vries, J., McCall, R., Van Dongeren, A., Zwinkels, C., Jacobs, R., 2010. XBeach: Non-hydrostatic model: Validation, verification and model description. Technical report. Delft University of Technology and Deltares, 59 pp.

Smith, G.A., Babanin, A.V., Riedel, P., Young, I.R., Oliver, S., Hubbert, G., 2011. Introduction of a new friction routine into the SWAN model that evaluates roughness due to bedform and sediment size changes. Coastal Engineering, 58, 317-326.

Stockdon, H.F., Holman, R.A., Howd, P.A., Sallenger, A.H., 2006. Empirical parameterization of setup, swash, and runup. Coastal Engineering, 53, 573-588.

Stockdon, H.F., Doran, K.S., Sallenger, A.H., 2009. Extraction of lidar-based dune-crest elevations for use in examining the vulnerability of beaches to inundation during hurricanes. Journal of Coastal Research, SI 53, 59-65.

Stone, G., Liu, B., Pepper, D. A., Wang, P., 2004. The importance of extratropical and tropical cyclones on the short-term evolution of barrier islands along the northern Gulf of Mexico, USA. Marine Geology, 210, 63-78.

Suter, J. R., Nummedal, D., A., Maynard, K., Kemp, P., 1982. A process-response model for hurricane washovers. Proceedings of 18th Coastal Engineering Conference, Capetown, South Africa, pp. 1459–1789.

van Dongeren, A., Roelvink, D., McCall, R., Nederhoff, K., van Rooijen, A., 2017. Modelling the morphological impacts of coastal storms. In: Coastal Storms: Processes and Impacts. (Ed.) Paolo Ciavola and Giovanni Coco, John Wiley & Sons Ltd., pp. 195-216.

Vila-Concejo, A., Matias, A., Ferreira, Ó., Duarte, C., Dias, J.A., 2002. Recent evolution of the natural inlets of a barrier island system in Southern Portugal. Journal of Coastal Research, SI 36, 741-752.

Vila-Concejo, A., Matias, A., Ferreira, Ó., Dias, J.A., 2006. Inlet sediment bypassing to a downdrift washover plain. Journal of Coastal Research, SI 39, 401–405.

Vousdoukas, M.I., Wziatek, D., Almeida, L. P., 2011. Coastal vulnerability assessment based on video wave run-up observations at a mesotidal, steep-sloped beach. Ocean Dynamics, 62(1), 123-137.